Investigating uncertainty and parameter sensitivity in bedform analysis by using a Monte Carlo approach

Julius Reich[1], Axel Winterscheid[1]

[1]Federal Institute of Hydrology, Department M3 – Fluvial Morphology, Sediment Dynamics and Management, Koblenz, 56068, Germany

Correspondence to: Julius Reich (reich@bafg.de)

Abstract. Precise and reliable information about bedforms, regarding geometry and dynamics, is relevant for many applications – like ensuring safe conditions for navigation along the waterways, parameterizing the roughness of the riverbed in numerical models, or improving bedload measurement and monitoring techniques. There are many bedform analysis tools to extract this information from bathymetrical data. However, most of these tools require the setting of various input parameters, which in turn influence the resulting bedform characteristics. How to set the values for these parameters and what influence they have on the calculations has not yet been comprehensively investigated. We therefore developed a workflow, to quantify this influence by performing a Monte Carlo Simulation. By repeating the calculations many times with varying input parameter settings, the possible range of results is revealed and procedure-specific uncertainties can be quantified. We implemented a combination of the widely used zerocrossing procedure to determine bedform geometries and a cross-correlation analysis to determine bedform dynamics. Both methods are well known and established, which ensures transferability and value of the findings. In order to increase the robustness of the workflow we decided to implement a wavelet analysis based on Bedforms-ATM (Guitierrez et al., 2018), which is carried out before the zerocrossing procedure. This provides further orientation and accuracy by identifying predominant bedform lengths in a given bed elevation profile. The workflow has a high degree of automation, which allows the processing of large amounts of data. We applied the workflow to a test dataset from Lower Rhine in Germany, which was collected by the Federal Waterways and Shipping Administration in February 2020. We found that bedform parameters reacted with different sensitivity to varying input parameter settings. For bedform heights uncertainties of up to 35 % and for bedform lengths uncertainties up to 50 % were identified. The setting of a window size in the zerocrossing procedure (especially for the superimposed small-scale bedforms in case they are present) was identified to be the most decisive input parameter. Here, however, the wavelet analysis offers orientation by providing a range of plausible input window sizes and thus allows a reduction of uncertainties. Concurrently, the time difference between two successive measurements has proven to have a significant influence on the determination of bedform dynamics. For the test dataset, the faster migrating small-scale bedforms were no longer traceable for intervals longer than two hours. At the same time, they contributed to up to 90 % of the total bedload transport, highlighting the need for measurements in high temporal resolution in order to avoid a severe underestimation.

1 Introduction

Bedforms are ubiquitous in rivers with sandy or gravelly beds (Carling et al., 2006; Kleinhans, 2001; Van Rijn, 1993). Their occurrence, shape and dimensions as well as their dynamics depend on hydraulic and morphological conditions. Knowing bedforms is crucial for various fields of application. For example, bedform crest heights influence the navigable depth along the waterways (e.g. Carling et al., 2006, Scheiber, Lojek, et al., 2021). This is why information about maximum bedform heights is required in order to ensure the safety and ease of navigation. From the perspective of hydraulics, bedforms increase the flow resistance at the river bed. In numerical modeling, bedform dimensions and shapes need to be parametrized and transformed into form roughness (Lefebvre and Winter, 2016; Venditti, 2013). The erosion of particles on the bedforms' upstream faces and the accumulation on their downstream faces result in a downstream movement of sediments, contributing to bedload transport (Simons et al., 1965). Therefore, bedload transport rates can be estimated based on bedform migration - so-called dunetracking (e.g. Claude et al., 2012; Leary and Buscombe, 2019; Simons et al., 1965) - representing an alternative approach to direct bedload measurements.

Over the years many tools were developed to derive both bedform geometries and migration rates from multibeam echosounding (MBES)-data (e.g. Cisneros et al., 2020; Gilja et al., 2016; Guitierrez et al., 2018; Henning, 2013; Lee et al, 2021; Lebrec et al., 2022; Lefebvre et al. 2022; Núñez-González et al., 2021; Ogor, 2019; Scheiber et al., 2021; Van der Mark and Blom, 2007; Van Dijk et al., 2008; Wang et al., 2020; Zomer et al., 2021a). Most of these tools require the setting of procedure-specific input parameters. Often, there are no theoretically sound criteria or anything like best practice for setting a specific value. For example, a widely used and established approach is the zerocrossing procedure, which is implemented in many published tools and has been used in many studies (e.g. Van der Mark & Blom, 2007, Leary and Buscombe, 2019, Wang et al., 2020; Zomer et al. 2021a). The identification of bedforms crests and troughs in a longitudinal bed elevation profile (BEP) is based on the calculation of a moving average, which requires the setting of a window size. However, there are no equations or guidelines for choosing a specific value. Therefore, the procedure is strongly influenced by the personal experience and subjective selection of the investigator. If applied by several investigators, different results will be obtained from the same procedure and for the same dataset. Despite the ubiquitous need to define the setting of these parameters, little attention has been paid on how different settings influence estimated bedform characteristics. A Monte Carlo Simulation (MCS) is a suitable approach to evaluate this influence of input parameter settings. An MCS is a computer based analytical method which utilizes sequences of random numbers as inputs into a model in order to obtain a probabilistic approximation to the solution (Adekitan, 2014). With regard to bedform analysis, repeated calculations with varying input parameters settings, reveal the possible range of results and enable robust estimates of the resulting bedform characteristics.

We therefore developed a workflow to perform extensive sensitivity and uncertainty analyses and applied it to a field dataset. The workflow includes an initial wavelet analysis, a zerocrossing procedure to determine bedform geometries and two different approaches to analyze bedform dynamics, which are partly based on existing tools. These individual steps are embedded in an MCS-routine to repeat the calculations with varying input parameter definitions. This is the key feature of the workflow and

65 allows to quantify the range of uncertainty for different bedform parameters (e.g. height, length, migration rate) due to the input parameter settings. Further on, it allows to compare the sensitivity of the different input parameters. Both can be of great value for future studies in order to estimate the uncertainty and the robustness of produced results.

The following aspects were decisive for the development of the workflow:

- **Uncertainty and sensitivity analyses:** The aim of the workflow is to investigate and quantify uncertainties and
70 sensitivities due to input parameter settings in bedform analysis by performing an MCS.

- **Automation:** Due to increasing data availability and the need for repeated calculations (within the MCS), we wanted to achieve a high degree of automation to enable a batch processing of large datasets. So, the algorithm was coded in a way that allows easy selection of multiple datasets and the performance of many iterations.

- **Transferability & value:** As mentioned earlier there are lots of different bedform analysis tools available. Each of
75 them is complex and it would be beyond the scope of this work to combine them within one comprehensive study. Therefore, we selected the well-established zerocrossing procedure to determine bedform geometries in combination with the cross-correlation analysis to determine bedform dynamics. Both approaches have been used in many studies or are even implemented in recently published tools (see list above). This way, value and transferability of the findings can be increased and there would be a larger group of potential users. With regard to bedform dynamics, we use the
80 zerocrossing procedure in combination with a newly introduced method as a second approach, which allows further validation and provides new insights into bedform dynamics.

- **Robustness:** Before the MCS can be carried out, a value range must be specified within which the input parameters are varied. In order to provide orientation and thus avoid diverging results, a wavelet analysis was added to the workflow based on Bedforms ATM (Guitierrez et al., 2018). This allows initial estimates about prevailing bedform
85 lengths in a given BEP, which is a required input parameter for the zerocrossing procedure. So, this way, the boundary conditions for the MCS can be defined and the accuracy and robustness of the procedure can be increased. The combination of wavelet analysis and zerocrossing procedure has already proven to be efficient in the algorithm developed by Wang el al. (2020). A further aim was to increase the robustness of the statistical evaluation of bedform characteristics. We therefore introduce a new parameter as a measure of total bedform height, which behaves more
90 robust compared to existing measures.

The entire workflow is based on the evaluation of longitudinal BEPs. Due to the high degree of automation large numbers of BEPs can be analyzed. By a dense arrangement of the individual BEPs, a spatial analysis can be approximated. We applied the workflow to a test dataset, which contains MBES-data of a 500 m stretch of the Lower Rhine in Germany. The data were
95 collected - during a three days campaign in February 2020 - by the Federal Waterways and Shipping Administration.

The method section introduces the implemented workflow and contains detailed descriptions of the individual steps and implemented methods. This is followed by a description of the MBES-dataset from Lower Rhine. In the results section the resulting bedform parameters and bedload transport rates are presented. The discussion section focuses on the interpretation

of the results as well as on the sensitivity of the different procedure-specific input parameters. Finally, the key findings are outlined in the conclusions section.

2 Method
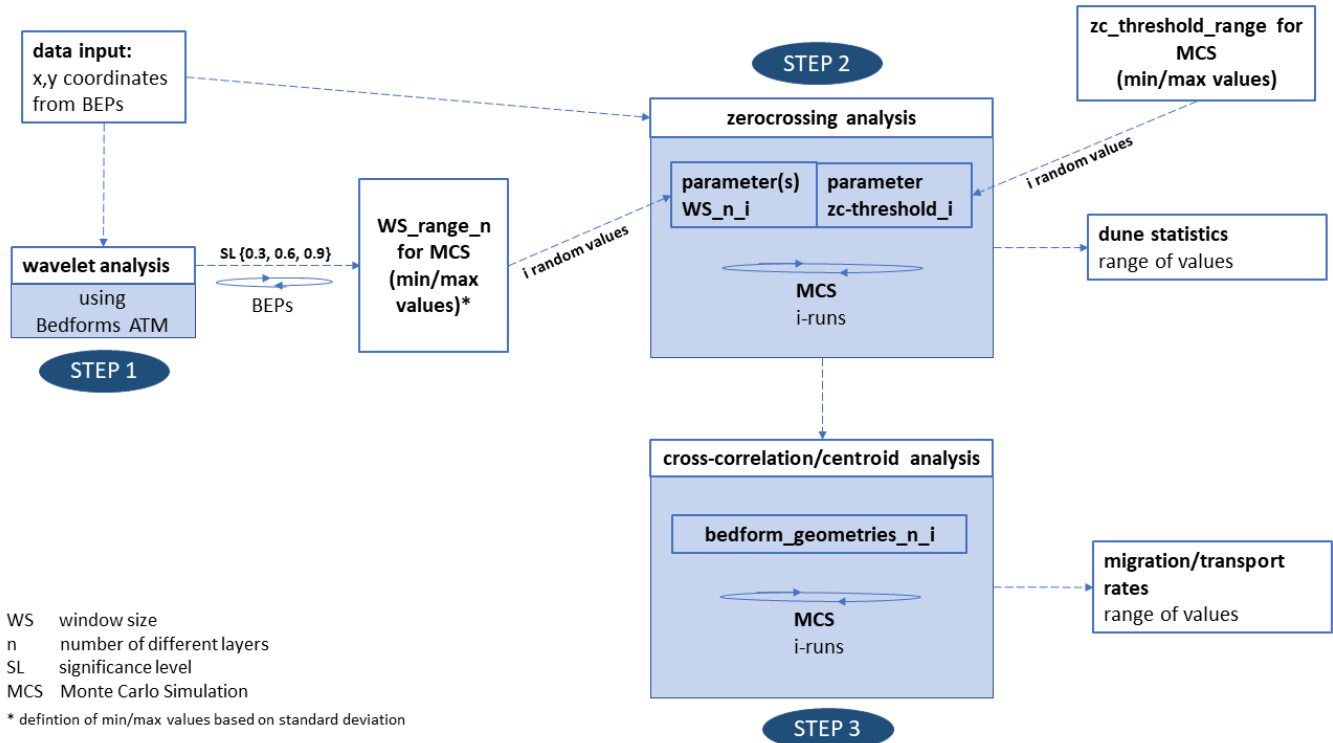
Figure 1: The implemented workflow consists of three steps. For considering the uncertainties associated with the setting of various input parameters, parts of the workflow are performed as an MCS.

Before describing the individual steps of the implemented workflow in detail, Figure 1 provides an overview for orientation. The workflow consists of the following key points:

- **Input data**: Longitudinal BEPs derived from MBES-data.
- **Step 1 – wavelet analysis**: Based on Bedforms-ATM predominant bedform lengths are identified in a given BEP by a continuous wavelet transform. This is a required input parameter for step 2.
- **Step 2 – zerocrossing:** The identified predominant bedform lengths are required input parameters (window sizes) for the zerocrossing procedure, based on the software RhenoBT (Frings et al., 2012), which is used to determine bedform geometries. By extending the original algorithm, a data export of tables containing information about individual bedform attributes (e.g. height, length, shape) was implemented, to enable extensive statistical analyses as an optional

post-processing routine. In addition, new statistical parameters for the characterization of bedform geometries were defined.

- **Step 3 – cross-correlation/centroid analysis:** Based on determined bedform geometries, bedform migration rates are calculated using a cross-correlation analysis or a newly introduced centroid analysis that detects the migration of the geometrical centroids of individual bedform areas. From a known migration rate bedload transport rates can be derived by considering grain density and porosity.

- **MCS:** At various points in the workflow the setting of input parameters is required. This has an impact on the results that is not immediately apparent to the user. Therefore, the calculations are repeated multiple times with different input parameter settings in order to reveal the range of plausible results and to evaluate the level of uncertainties.

2.1 Preprocessing & data preparation

Before the actual analysis, the spatial discretization of the river section under investigation has to be defined. Spatial discretization lateral to the flow direction is given by the distance between the BEPs to each other. The more heterogeneous the investigated bedform field (high spatial variation of bedform dimensions), the denser the arrangement of BEPs should be. In longitudinal direction a division into subsections is mandatory. Later, the statistical parameters (e.g. the average bedform height and length) are calculated per subsection (see section 2.4).

In order to obtain the BEPs from the MBES-data, some hydrographic preprocessing steps are required. Based on the plausibilized raw MBES-data, a geometric modeling is suitable to reduce included measurement uncertainties. For this purpose, the measurement data is gridded and for each grid point, a polynomial is approximated to the 3D point cloud within a given radius. In case of the test dataset from Lower Rhine, a surface approximation with polynomials using least squares fit was applied. Along the considered profile tracks the individual BEPs are derived from the DEMs. A detailed description of hydrographic preprocessing steps can be found e.g. in Lorenz et al. (2021a).

2.2 Wavelet analysis

The first step of the workflow is a continuous wavelet transform based on Bedforms-ATM. It is performed to identify the predominant wavelengths (interpreted as bedform lengths) in the individual BEPs. The predominant bedform lengths are required input parameters for the zerocrossing procedure that follows in the second step. Wavelet transforms have been used in a variety of applications to analyze riverbed roughness (Nyander et al., 2003) or to discriminate engineering surfaces (Raja et al., 2002). Compared to Fourier methods they are more suitable for signals containing discontinuities. In terms of bedform analyses the so-called Morlet wavelet has appeared to be the most efficient (Guitierrez et al., 2018) and has been used for all analyses in this study. As a result of the wavelet transform, a spectrum is obtained, which indicates the dominance of individual wavelengths in a BEP. Figure 2 shows the so-called wavelet power spectrum for an exemplary BEP excerpt. Based on the chosen significance level, the predominant wavelengths are identified. Only those peaks in the wavelet power spectrum that are greater than the global significance are considered. By default, the significance level has to be set by the user. In the shown

example (Figure 2) three different significance levels lead to three different results. Accordingly, the workflow has been adapted, so that the analysis is executed three times for each BEP with significance levels of 0.3, 0.6 and 0.9. If two predominant wavelengths (equal to two individual peaks included in the wavelet power spectrum) have been detected, it is assumed that two coexistent layers of bedforms are present. For example, small-scale secondary bedforms might be migrating over large-scale underlying bedforms with (likely) higher migration rates (e.g. Carling et al., 2006; Gilja et al., 2013; Kleinhans et al., 2002).

The resulting wavelengths from all analyzed BEPs are stored in a table. This table contains the total number of detected wavelengths and is passed to the next step in the workflow (zerocrossing procedure) after outliers have been removed. For this purpose, mean value and standard deviation σ are calculated for each detected bedform layer. Values that lie outside the range of $\pm 2\sigma$ around the mean value are removed. Nevertheless, before carrying out the further calculation steps, it is recommended to check the results from the wavelet analysis for plausibility, to compare them with site-specific knowledge about occurring bedform dimensions and to make manual adjustments if necessary. The most sensitive step is deciding on the number of bedform layers representing features with predominant wavelengths. Due to potential ambiguity of the results, this step is not automated but requires a critical assessment based on the present morphological conditions. In the example shown in Figure 2 different significance levels indicate a different number of bedform layers for the same BEP. In the first case (Figure 2b), two bedform layers are detected with wavelengths of 8 m and 26 m. In the second case (Figure 2c), two bedform layers are detected with wavelengths of 8 m and 23 m. In the third case (Figure 2d), only one layer with a wavelength of 8 m is detected because the second peak is below the global significance. This decision has a great impact on all analyses that follow (in a recently published meta-analysis by Scheiber et al. (2024), in which five bedform analysis algorithms were compared, the consideration of a second bedform layer was also identified as the most significant cause of deviations between the results of the different algorithms). For instance, the estimated bedload transport rates at the end of the procedure can be over- or underestimated based on the selected number of bedform layers. To make this decision, a visual inspection of the BEPs is recommended. In addition, the calculation of bedform migration rates can be used as validation. If migration rates with high correlation coefficients can be detected for both bedform layers, it can be assumed that the number of layers has been chosen correctly.

Optionally - especially in case of larger-scale gradients of the channel bed (e.g. due to underlying bars) - a detrending of the BEPs can be performed, using robust-spline filter techniques. The algorithm is based on a discrete cosine transform and is used to smooth the initial signal. The degree of smoothing depends on the adjustable s-parameter (for further information refer to Guitierrez et al., 2013).
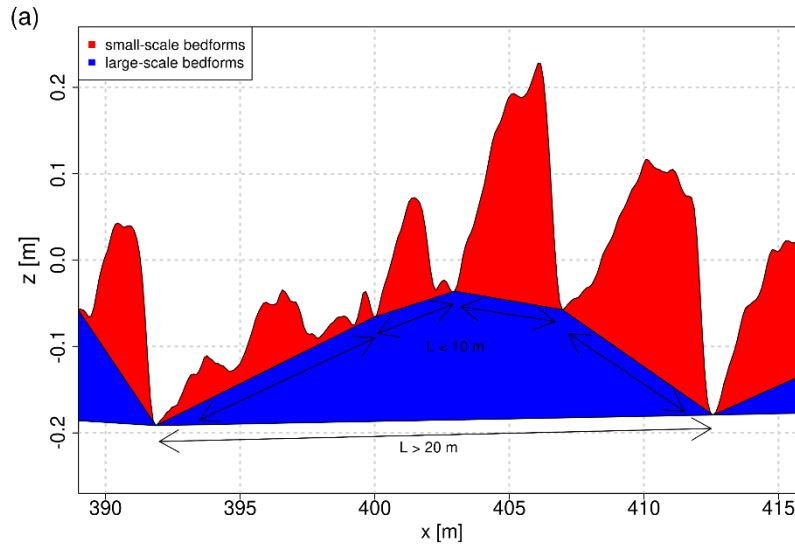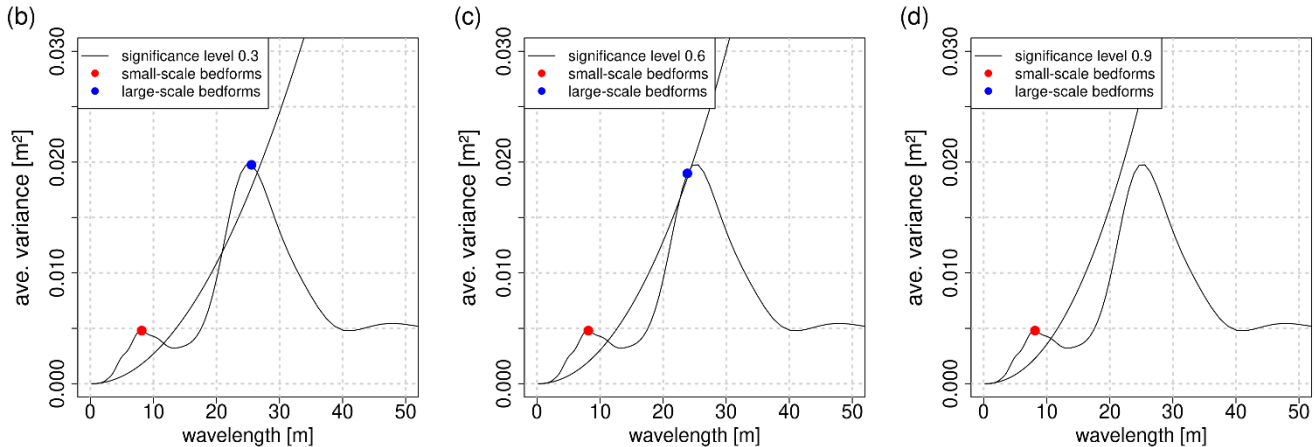
Figure 2: Identifying predominant wavelengths of a BEP by means of wavelet analysis: Depending on the chosen significance level different wavelengths are identified. (a) - Excerpt of an exemplary BEP of the test dataset from Lower Rhine separated into two layers of bedforms. (b-d) – Identified predominant wavelengths by means of wavelet analysis with a significance level of 0.3, 0.6 and 0.9. In the first two cases (b, c) two layers of bedforms are identified. In the third case (d) only one layer of bedforms is identified.

2.3 Zerocrossing procedure

The zerocrossing procedure is adapted from the software RhenoBT, respectively the bedform tracking tool by Van der Mark and Blom (2007). It is a widely used approach for analyzing BEPs with respect to bedform geometries (see section 1). Herein a moving average is calculated over the considered BEP by setting a window size. Ideally, the chosen window size should

185 approximately correspond to the expected bedform length. For this reason, the results from step 1 (wavelet analysis) provide the rationale for setting the adequate window size. Figure 3 illustrates the procedure. Based on the moving average the zerocrossings are calculated. The local minima between each two zerocrossings are interpreted as bedform troughs. To limit the effect of small-scale fluctuations in the BEPs a zc-threshold is used, which defines the minimum distance between a bedform trough and the moving average. Only local minima with distances larger than the zc-threshold are considered. There

190 is no objective criteria for its exact definition, but globally, it must not be greater than the minimum expected bedform height. At the end of the procedure, one or two (depending on the selected number of bedform layers) baselines are constructed that separate the individual bedform layers from each other. The lowest baseline separates the bedforms from the non-active layer of the river bed. Based on this separation the individual bedform attributes (height, length and shape) are calculated. If two bedform layers are present, the individual attributes are calculated for each layer separately. In such a case the baseline of the

195 small-scale bedforms is calculated first (Figure 3a). Then, the procedure is repeated by calculating the moving average - with the corresponding window size for the underlying large-scale bedforms - over the previously calculated baseline of the small-scale bedforms (Figure 3b).
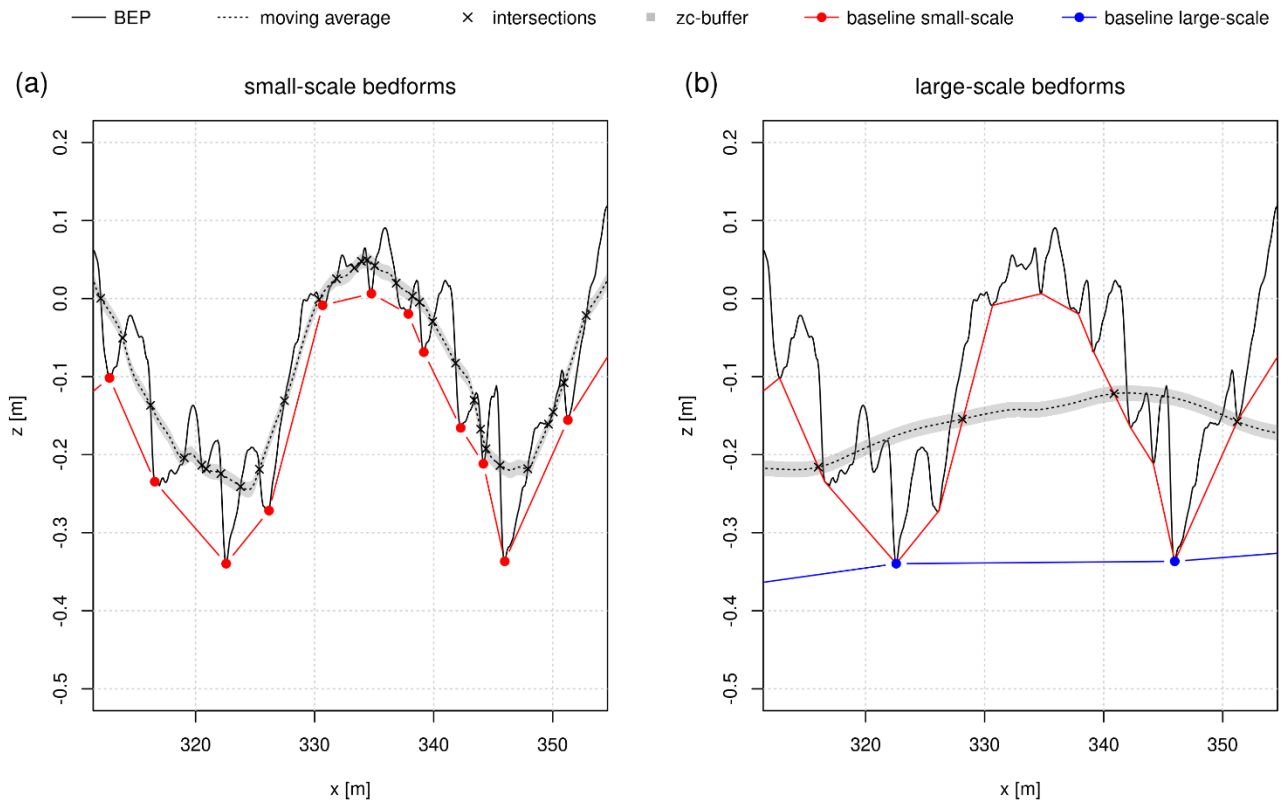
200 **Figure 3: Zerocrossing procedure. (a) - Calculation of the baseline of the small-scale bedforms. (b) - Calculation of the baseline of the large-scale bedforms.**

2.4 Bedform statistics

The results of the zerocrossing procedure can be exported as tables, which summarize geometric attributes for each individual bedform as well as the chosen input parameter settings (Table 1), e.g. to enable subsequent statistical analyses as a post-processing routine. The tables are exported for each BEP, subsection, bedform layer and iteration of the MCS.

Table 1: Output from the analysis containing geometrical attributes for each bedform layer

attribute	definition
x-position [m]	x-position along the BEP
length [m]	bedform length
height [m]	bedform height
points [-]	number of points
area [m²]	exact bedform area
shape factor [-]	relation between the exact bedform area and the area of the triangle formed by two adjacent bedform troughs and the bedform crest
layer [-]	related bedform layer
iteration [-]	iteration within MCS
windowsize [m]	selected window size
zc-threshold [m]	selected zc-threshold

In accordance to the definition of individual attributes described in Wesseling & Wilbers (2000), bedform length is defined as the length of the line connecting two adjacent troughs, while bedform height is the height of the triangle formed by a crest and its two adjacent troughs. Total height H_{total} is determined by measuring the height of the triangle which is defined by two adjacent troughs of the large-scale bedforms and the maximum of the BEP in between (see Figure 4a). Total length L_{total} is equal to the length of the large-scale bedforms. The shape factor S (-) is the relation between the exact bedform area and the simplified bedform area resulting from the triangle formed by bedform height and length (Ten Brinke et al., 1999).

$$S = \frac{A}{0.5 \cdot H \cdot L} \tag{1}$$

Based on these individual bedform attributes, statistical parameters are calculated to describe average bedform characteristics in a defined subsection of the BEP. For this purpose, the median is formed over all individual bedform attributes contained in a subsection. Since the determination of these parameters results from the averaging of individual attributes, their significance depends on the number of detected bedforms in the considered subsection. For this reason, another parameter for estimating the total bedform height was implemented, which is independent of the number of identified bedforms. For obtaining the so-called T90-parameter, in each x-value the vertical difference between lowest baseline and the BEP is calculated (see Figure 4b). Finally, the 90 % percentile of the resulting values is formed within each subsection. The parameter is therefore not based on measuring the height of individual bedforms but on measuring the accumulated bedform layer thickness (T) along the entire

BEP. The 90 % percentile approximately corresponds to the average total bedform height of individual bedforms in a
225 subsection. This means that both T_{90} and H_{total} are used to quantify the same property, but T90 is expected to behave more
robust due to the mentioned aspects. Table 2 summarizes the definition of the different parameters.
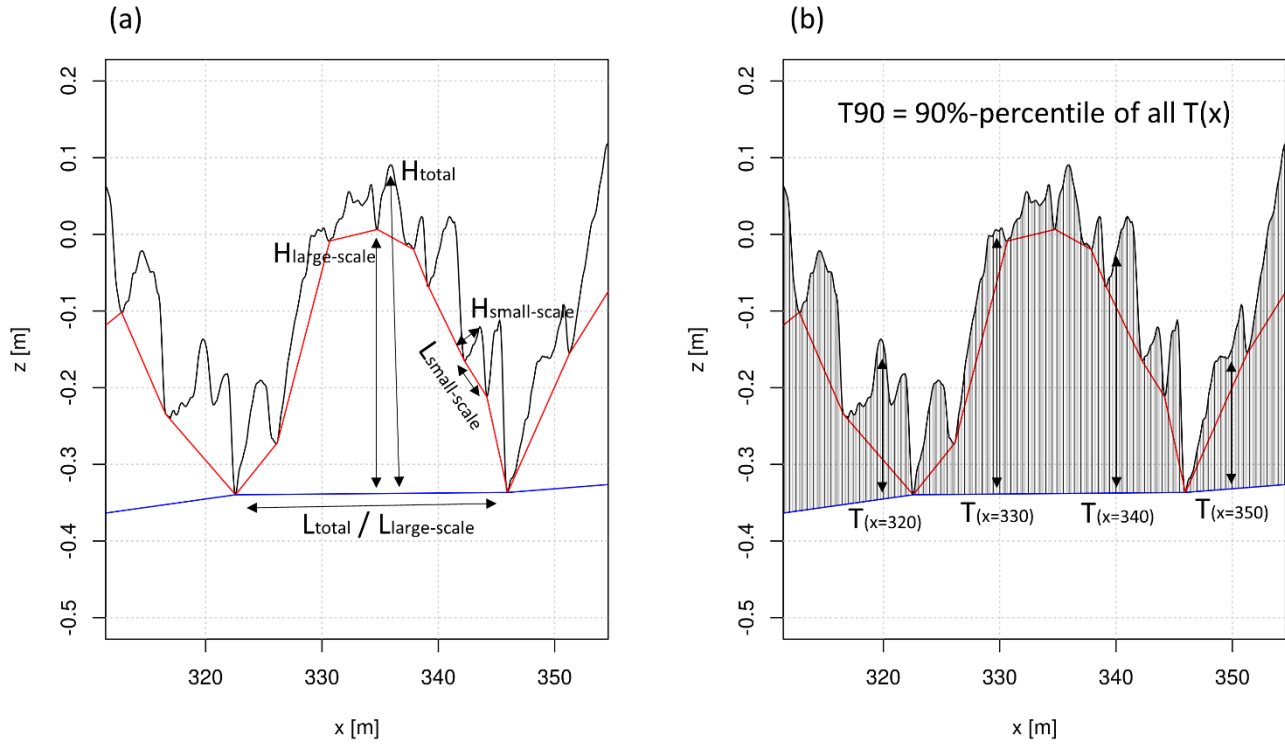
Figure 4: (a) – Definition of individual bedform attributes. (b) – Determination of the T90-parameter.

230 Table 2: Definition of bedform parameters.

parameter	Definition	description
T90	90 % percentile of all T(x) along subsection with distance dx	Measure for average total bedform height in a subsection.
H_{total}	Median of all $H_{total}(i)$ in a subsection	Measure for average total bedform height in a subsection.
$H_{small\text{-}scale}$	Median of all $H_{small\text{-}scale}(i)$ in a subsection	Measure for average small-scale bedform height in a subsection.
$H_{large\text{-}scale}$	Median of all $H_{large\text{-}scale}(i)$ in a subsection	Measure for average large-scale bedform height in a subsection.
$L_{small\text{-}scale}$	Median of all $L_{small\text{-}scale}(i)$ in a subsection	Measure for average small-scale bedform length in a subsection.

$L_{large\text{-}scale}/L_{total}$	Median of all $L_{large\text{-}scale}(i)/L_{total}(i)$ in a subsection	Measure for average large-scale/total bedform length in a subsection.

2.5 Estimation of bedform migration & bedload transport

Bedform migration rates can be determined if consecutive measurements over time are available. For this purpose, two different methods were implemented. By means of a cross-correlation analysis the spatial offset between two consecutive

235 BEPs is identified (Leary and Buscombe, 2019; McElroy and Mohrig, 2009; Van der Mark and Blom, 2007). With the known time difference between each two measurements, migration rates are determined. They can be estimated for the total BEP as well as for the individual bedform layers by using the constructed baselines from the zerocrossing procedure. This can be a decisive aspect in case bedforms of different dimensions occur that migrate with different rates. As many different solutions emerge from the MCS for constructing the baselines (because different input parameter settings are used), the cross-correlation

240 analysis is also carried out as an MCS. So, many iterations are performed with different baselines for the same BEP. To consider the small-scale bedforms of the upper layer separately, the upper baseline is subtracted from the initial BEP. The resulting geometries represent the isolated small-scale bedforms and are subsequently used in the cross-correlation analysis. To consider the large-scale bedforms of the lower layer, there are two possible approaches which were evaluated before the final implementation. The first approach is based on a subtraction of the lower baseline from the upper baseline. However,

245 preliminary results (not shown here) indicate that correlations are relatively low for this approach. Another option is to directly use the upper baseline in the cross-correlation analysis. Both approaches lead to an isolated representation of the large-scale bedforms. The second approach proved to be more suitable, as higher correlations could be achieved here and was therefore implemented.

In addition to the cross-correlation analysis an alternative method has been developed to better determine the migration rates

250 of the small-scale bedforms. The migration of smaller superimposed bedforms decisively contributes to total bedload transport. The resulting quantity may even exceed the transport associated with larger underlying bedforms (Zomer et al., 2021b). This highlights the need for a more detailed analysis of this process. In the presented method, individual migration rates are obtained - instead of an average migration rate along the entire BEP - by tracking the geometric centroids of individual bedform areas. For two consecutive measurements geometric centroids are calculated for all individual bedform areas obtained from the

255 zerocrossing procedure. Each centroid from the first measurement is assigned to the centroid from the second measurement with the smallest distance in downstream direction. The offset between each pair of centroids corresponds to the individual migration distance. By knowing the time difference between both measurements, migration rates are determined. In order to ensure a correct assignment of corresponding centroids some plausibility check criteria have been defined. For each pair of bedforms, the ratio of bedform length ($L(t2)/L(t1)$) and bedform area ($A(t2)/A(t1)$) is calculated. To ensure a reliable

260 assignment, a threshold allowing 25 % of deformation (concerning length and area) was set. All pairs of bedforms whose ratios exceed this threshold are excluded. This means that bedforms, whose shape has already changed too much to allow a reliable

assignment are not included in the further analysis. The obtained results provide insights into the variability of bedform migration rates along a BEP and can be related to specific geometric attributes. To derive a weighted average migration rate (c_m) from the individual rates for a considered BEP, the products of individual migration rate (c_i) and corresponding bedform length (L_i) are summed up and divided by the total length of the BEP (L_{BEP}).

$$c_m = \frac{\sum c_i \cdot L_i}{L_{BEP}} \tag{2}$$

Like the cross-correlation analysis, the centroid analysis is also carried out as an MCS by using the various bedform geometries determined in step 2.

Figure 5 illustrates the two methods for a pair of BEPs selected for demonstration purpose. Figure 5a shows the results from the cross-correlation analysis and the shifted BEPs. Figure 5b shows the calculated individual offsets from the centroid analysis. In the following, the cross-correlation analysis is referred to as method 1 and the centroid analysis as method 2.
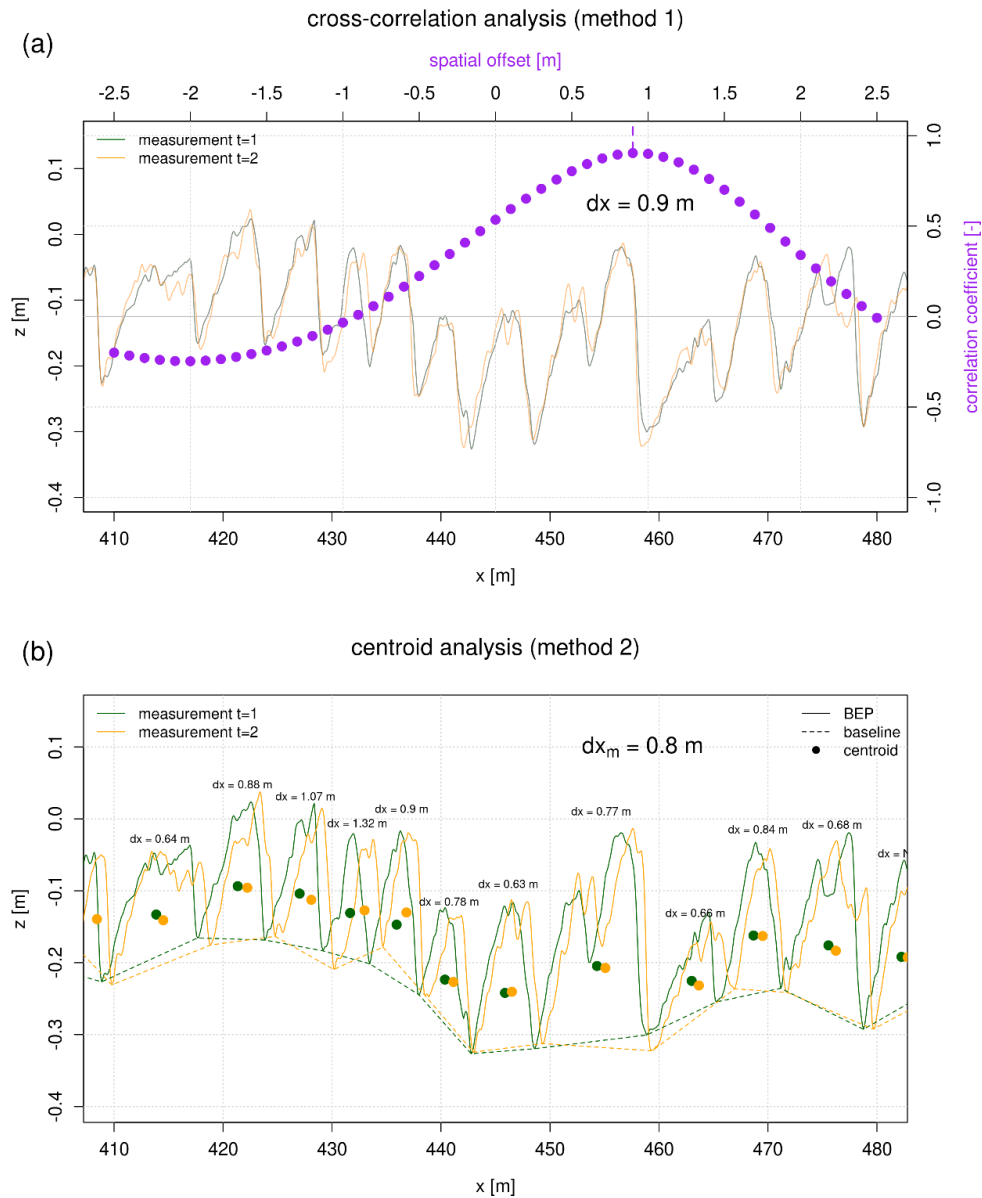
Figure 5: Calculation of bedform migration based on the cross-correlation analysis (a) and by comparing the geometrical centroids individual bedform areas (b). The time difference between both measurements was 0.4 h.

Based on the obtained migration rates - and by considering porosity and density, bedload transport rates (given in g s^{-1} m^{-1}) can be estimated. The approach by Ten Brinke et al. (1999) includes migration rate c (m s^{-1}), density ρ (g cm^{-3}), porosity n (-), bedform height H (m) and shape factor S (-).

$$q_b = c \cdot H \cdot S \cdot 0.5 \cdot \rho \cdot (1 - n) \qquad \textbf{(3)}$$

Since during the procedure the exact area of each single bedform is calculated, shape factor and bedform height can be replaced. For this purpose, the sum A (m²) of the individual bedform areas is used. This way, no averaging of bedform characteristics along the BEP is necessary. To obtain the correct unit, the result must be divided by the total length of the BEP.

285

$$q_b = c \cdot \frac{A}{L_{BEP}} \cdot \rho \cdot (1 - n) \qquad \textbf{(4)}$$

The calculation of bedload transport is also part of the MCS as the results depend on the obtained bedform geometries and migration rates.

2.6 Monte Carlo simulation

290 According to Figure 1, steps 2 and 3 of the developed workflow are executed as an MCS in order to address the possible range of results and the correspondent level of uncertainty. Concerning step 1, the results of the wavelet analysis provide an orientation for setting the window sizes in step 2 (zerocrossing procedure). For each BEP, the wavelet analysis is performed three times with significance levels of 0.3, 0.6 and 0.9. The resulting bedform lengths from all analyzed BEPs are stored in a table. This table now contains the total number of detected bedform lengths. In order to exclude outliers, mean value and

295 standard deviation σ are calculated for each layer. The final range of considered bedform lengths for each layer results from ± 2σ around the mean value (denoted as 'WS_range_n' in Figure 1). These steps ensure an automated and a reproducible procedure. The obtained ranges of bedform lengths are then used in the following zerocrossing procedure.

For applying the zerocrossing procedure in step 2, the user-defined inputs are the following parameters: i) the respective *window sizes* for calculating the moving average of the individual bedform layers (denoted as 'WS_n_i' in Figure 1), and ii)

300 the *zc-threshold* (denoted as 'zc-threshold_i' in Figure 1). Within a given range, random values are generated for each parameter according to a uniform distribution. Concerning the *window sizes*, the ranges of bedform lengths resulting from the wavelet analysis are used ('WS_range_n_for MCS'). For *zc-threshold* there is a lack of objective criteria, but globally, it must not be greater than the minimum expected bedform height. The random values for i) und ii) are generated once and are then used for all BEPs and all repeated measurements, in order to ensure comparability. Using all available sets of generated random

305 values results in multiple representations of the bedform geometries for each BEP (denoted as 'bedform_geometries_n_i' in Figure 1). All these representations are then used to calculate bedform migration and bedload transport rates in step 3, in which two consecutive measurements over time are always considered in pairs. To ensure comparability, only pairs of representations of the bedform geometries with identical parameter settings are considered.

By performing this MCS, the possible range of results can be quantified for all steps of the procedure. At the same time, the

310 various statistical parameters can be examined with respect to their robustness. For examining the behavior of each input

parameter separately, additional runs can be executed in which only one parameter is varied at a time while all the other parameters are kept constant. The number of iterations is freely selectable. The higher the number the more robust the estimates. On the other hand, a very high number of iterations leads to longer computational times. With respect to the analyses shown here, 100 iterations per BEP were performed.

3 Dataset

The developed workflow was applied to an MBES-dataset from Lower Rhine in Germany. The dataset was obtained during a field measurement carried out by the German Federal Waterways and Shipping Administration in February 2020. All hydrographic processing steps (e.g. plausibility checks, geometric modelling, extraction of longitudinal BEPs from spatial data) were carried out by the Federal Institute of Hydrology.

The study area is located close to Emmerich at Rhine-kilometer 860.0 to 860.5 and covers 500 meters in length and about 200 meters in width (see Figure 6). The section is characterized by a mixed sand and gravel bed with grain sizes in the order of 6 mm (D50). According to BfG (2011) grain density was assumed to be 2.603 g cm^{-3} and for porosity a value of 0.30 was selected. The measurements were taken on consecutive days at medium to high flow conditions with discharges ranging from 4000 to 4200 m³ s^{-1} at gauging station Emmerich (long term mean discharge at 2260 m³ s^{-1}) and depth-averaged flow velocities of about 1.9 m s^{-1} in the main channel. There was a peak in discharge ten days before the first day of the campaign exceeding a discharge of 6000 m³ s^{-1}. The total area covered with bedforms was measured four times with intervals between three and 24 hours. Additional MBES-data were collected along a single measurement swath in the center of the bedform field at shorter intervals, allowing a more detailed analysis of bedform migration and bedload transport. All measurements were collected using a Kongsberg Maritime multibeam echosounder EM3002 combined with the positioning by a Trimble antenna SPS185 in PDGPS mode, an estimation of heading by a Seapath 330 system and an inertial measurement unit (MRU5+). Beam footprints can be quantified in the range of 0.09–0.27 m for a typical depth of 3.5 m and a beam divergence of 1.5∘ × 1.5∘. The point cloud density is about 330 points per m2 and the measurement uncertainty regarding the elevation of a single point can be specified by 0.15 m (95 % confidence level).

Table 3 shows all measurements performed during the campaign. In order to expand the data basis with respect to bedform migration and bedload transport, not only directly consecutive measurements but all possible combinations (for dt > 0) are considered. The 10 available detailed measurements thus result in $\binom{10}{2} = 45$ possible combinations (see Appendix A).
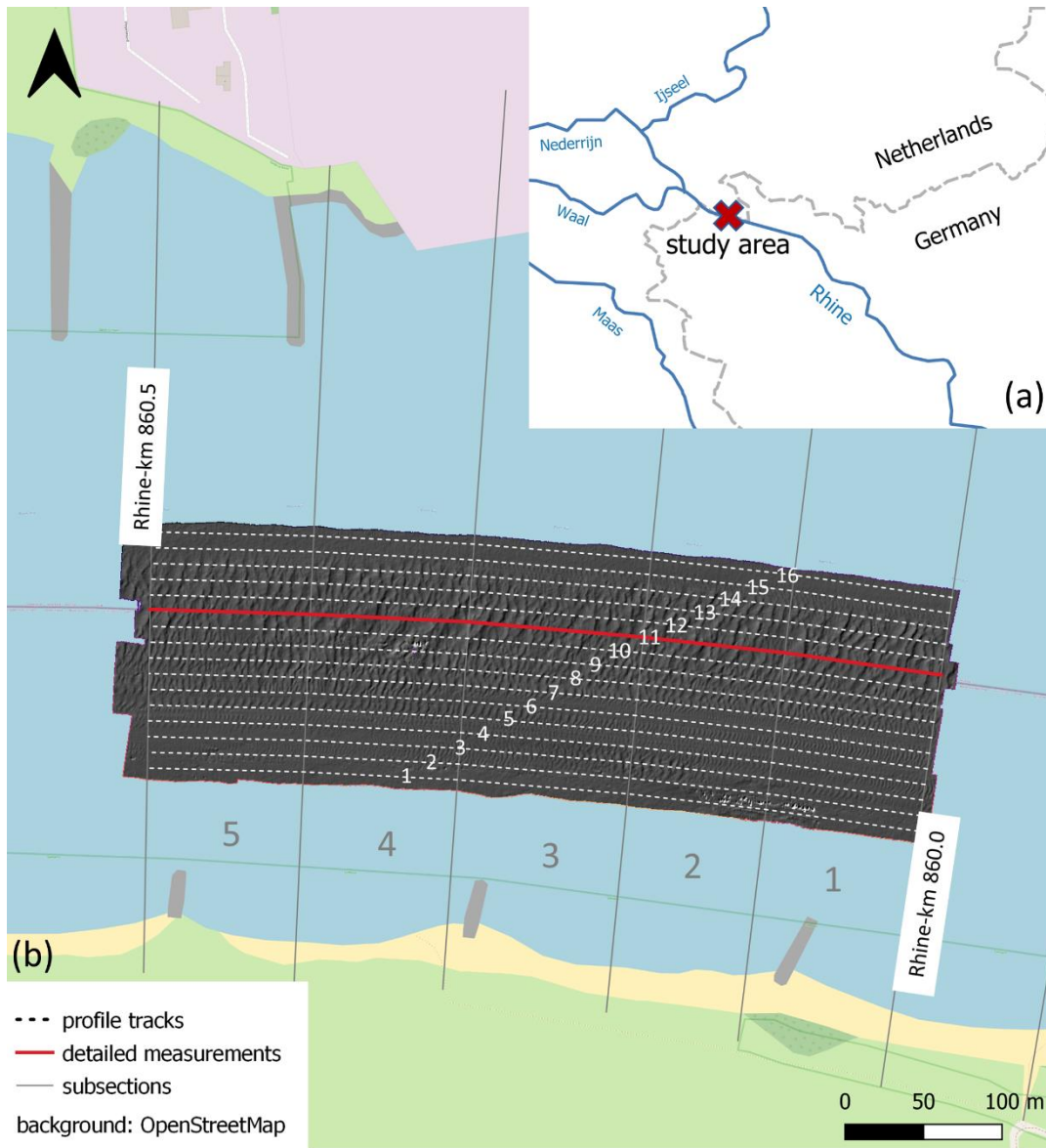
Figure 6: Study area near Emmerich (Rhine-km 860.0 to 860.5). Spatial discretization into 16 profile tracks lateral to flow direction and into 100-meter subsections in longitudinal direction. Base map is from © OpenStreetMap contributors 2023. Distributed under the Open Data Commons Open Database License (ODbL) v1.0.

Table 3: Performed MBES-measurements during the field campaign.

No.	date	time (MET)	measured area	Δt [h][1]
1	17 February 2020	09:35–10:41	total bedform field	-
2	18 February 2020	09:35–10:21	total bedform field	24.0
3	18 February 2020	12:48–13:31	total bedform field	3.2
4	19 February 2020	09:52–10:36	total bedform field	21.1
5	17 February 2020	11:17–11:24	center	-
6	17 February 2020	12.13–12:20	center	0.9
7	18 February 2020	08:46–08:54	center	20.6
8	18 February 2020	10:29–10:37	center	1.7
9	18 February 2020	10:41–10:48	center	0.2
10	18 February 2020	11:05–11:13	center	0.4
11	18 February 2020	11:57–12:04	center	0.9
12	18 February 2020	13:36–13:43	center	1.6
13	19 February 2020	09:24–09:32	center	19.8
14	19 February 2020	11:12–11:20	center	1.8

345

Hydrographic processing was performed according to Lorenz et al. (2021a). The measurement data were plausibilized and modelled to a regular grid with a point spacing of 10 cm by a surface approximation with polynomials using least squares fit. By triangular meshing of the DEM longitudinal BEPs were derived. The measured bedform field was subdivided into 16 BEPS with a lateral distance of 10 m to each other (see Figure 6b). Starting from the left boundary of the navigation channel, the

350   profile lines were shifted parallel as a polyline in specific intervals so that all profile lines were parallel and equidistant (10 m) to each other. Figure 7 shows the derived BEPs. Largest bedforms are located between BEP 8 and BEP 14 covering the entire length of the study area. Between BEP 3 and BEP 7 smaller bedforms are located, occurring only occasionally in individual subsections. Along BEP 15 and 16 no significant bedforms were measured. A macro structure is recognizable, particularly in BEPs 1 to 4. It extends from the head of the groyne on the left bank to the middle of the channel. The length of the structure

355   exceeds that of the longest other bedforms by an order of magnitude. By analyzing the collected MBES-data no migration of the structure could be identified within 48 hours. We therefore assume that this is not a migrating bedform, but an accumulation of sediments that were washed out between the groynes during the previous flood event. The geometry, with a steep stoss side

---

[1] time difference to previous measurement

and a flat lee side, is also contrary to the conditions typically found for downstream migrating bedforms. Further on, even if the structure was migrating, the time difference between the measurements would not be sufficient to analyze its migration rate. This is why we decided, not to include it in the analyses shown in section 4.2.
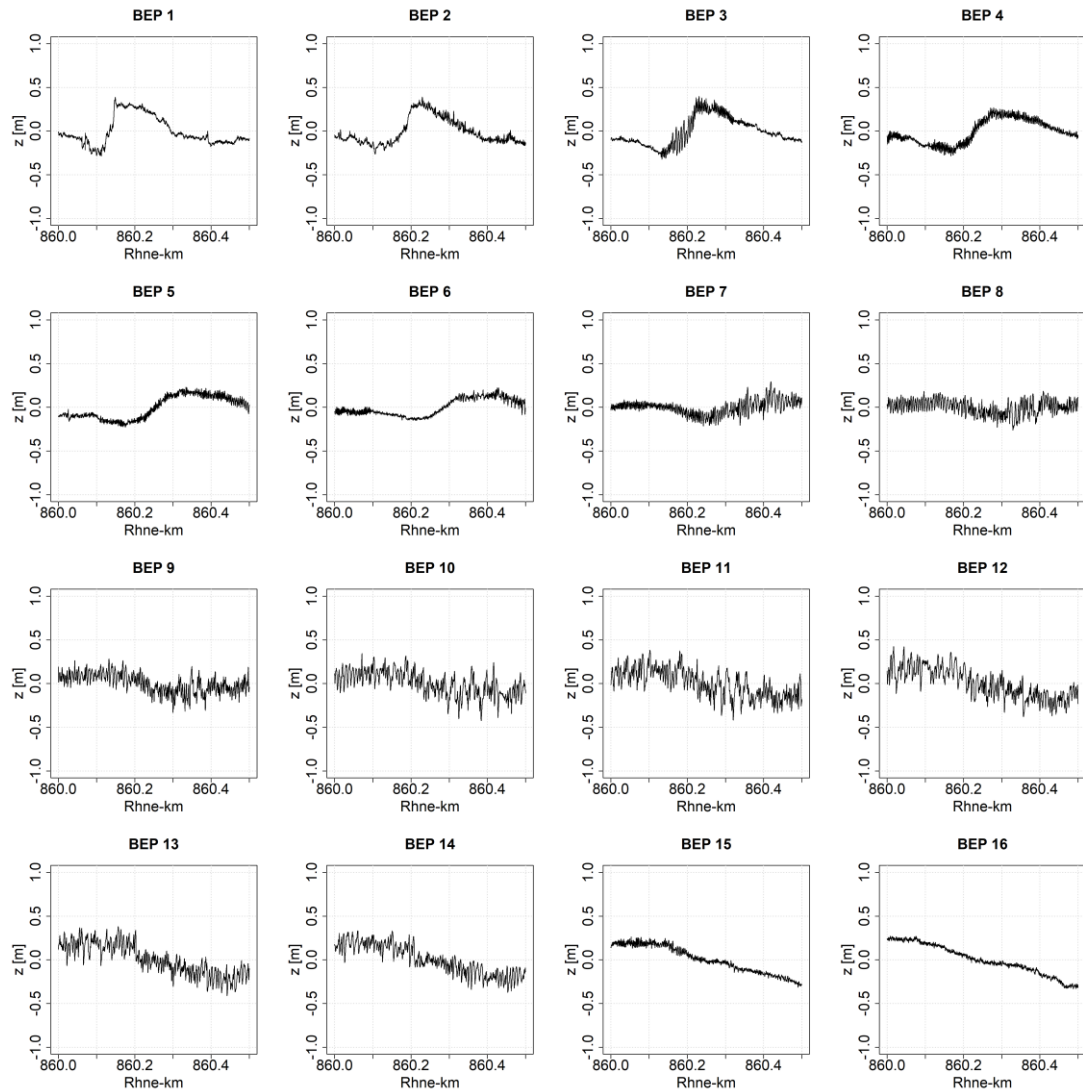
Figure 7: BEPs derived from MBES-data of the first measurement from 17 February 2020.

4 Results

4.1 Wavelet analysis

Figure 8 shows the identified predominant wavelengths calculated in the first step (wavelet analysis based on Bedforms-ATM). Wavelengths of the small-scale bedforms slightly increase from left to right reaching a maximum of 13 meters. Near the boundaries of the study area no wavelengths could be identified (BEPs 1 & 2 as well as 15 & 16). In the center of the bedform field, a second layer of large-scale bedforms with wavelengths in the order of 25 meters was detected. A visual comparison of the results with the BEPs shown in Figure 7 confirms the plausibility of the results. The resulting migration rates from the cross-correlation analysis (see section 4.3) will also verify the assumption of two separate layers. The detected wavelengths are based on all four measurements of the total bedform field (see Table 3) and on different settings of the significance level which were 0.3, 0.6 and 0.9.

In the further analyses only the center of the bedform field (BEP 8 to 14) was considered. Along the other BEPs, either only very small bedforms occur or bedforms only cover a limited section. The ranges of respected wavelengths are defined by twice the standard deviation around the mean value (see Sect. 2.2). All detected wavelengths were within the specified ranges.
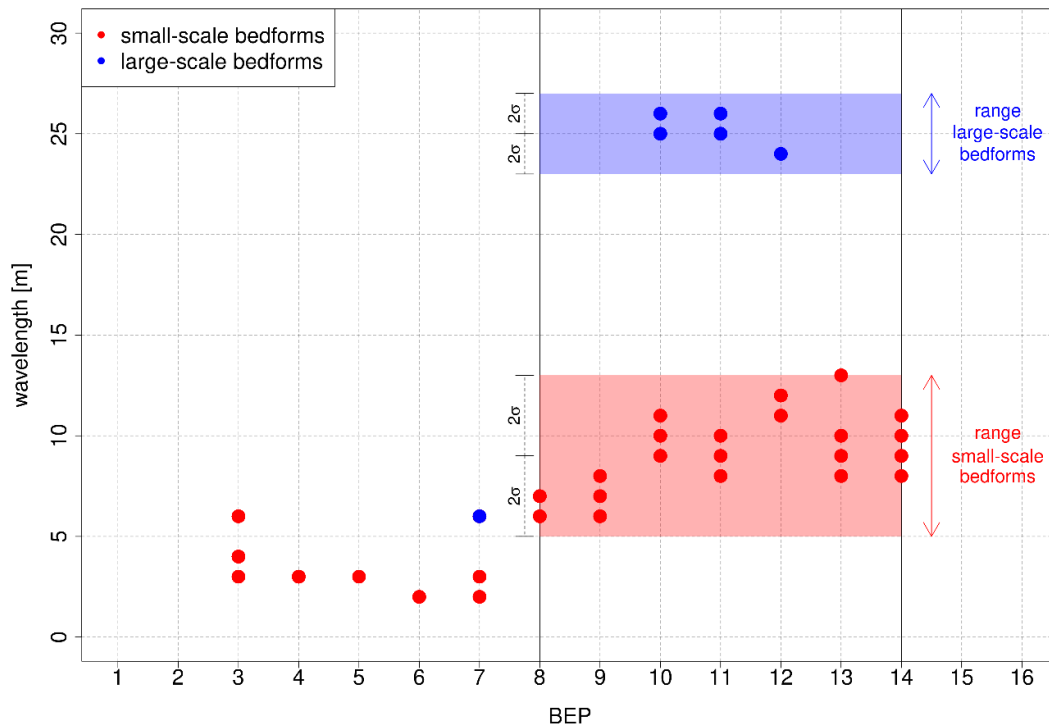
Figure 8: Derivation of the ranges of window sizes for the zerocrossing procedure from the identified predominant wavelengths in individual BEPs by means of wavelet analysis.

4.2 Bedform geometries

The wavelet analysis determines the range of values for the input parameter *window size* in the zerocrossing procedure (step 2). For each BEP, 100 iterations were performed with varying settings (MCS). *Window sizes* for small-scale bedforms were varied between five and 13 meters while *window sizes* for large-scale bedforms were varied between 23 and 27 meters (according to ± 2σ in Figure 8). The setting of *zc-threshold*, the second input parameter, was varied between 0.5 and 5 cm, which are assumed to be smaller values than the expected minimum bedform height. At the same time, the derivation of even smaller structures would reach the limits of measurement accuracy. Based on the specified ranges for each input parameter, random values are generated according to a uniform distribution. Figure 9 shows the bedform parameters obtained from 100 iterations. The parameters were averaged along each BEP. With respect to bedform geometries temporal changes can be neglected due to the short time differences between the individual measurements. Therefore, only the first measurement (no. 1 in Table 3) is considered in this context.

Regarding total bedform height, the T90 parameter remains nearly constant over all iterations for all BEPs, whereas the H_{total}-parameter has a higher scattering with a maximum range of about 5 cm (Figure 9a/b). The mean for both parameters takes a maximum in BEP 11 (values of 33 and 35 cm). Considering the individual bedform layers (Figure 9c/d), the large-scale bedforms appear to be slightly lower (mean values range from 15 cm to 19 cm for the small-scale bedforms and from 5 cm to 15 cm for the large-scale bedforms) but much longer than the identified small-scale bedforms (mean values range from 5 m to 6 m for the small-scale bedforms and from 17 m to 22 m for the large-scale bedforms). Bedform lengths appear to behave very sensitive with respect to varying input parameter settings. Lengths of the small-scale bedforms have a maximum total range of 4 m while lengths of the large-scale bedforms have a maximum total range of up to 10 m in BEP 14. It should be noted that spatial averaging (over the cross section) can lead to a stabilization and thus to a decreased scattering of the results, which is shown in (Figure 9e). The relative ranges ((max-min)/mean) of the individual parameters are shown here, which were averaged over the BEPs no. 8-14. By far the lowest values are found for the total bedform height (values of 2 % for T_{90} and 10 % for H_{total}). Individual bedform heights show much higher values between 30 % and 35 %. Highest values, however, are found for bedform lengths with a value of almost 50 % for the small-scale bedforms.
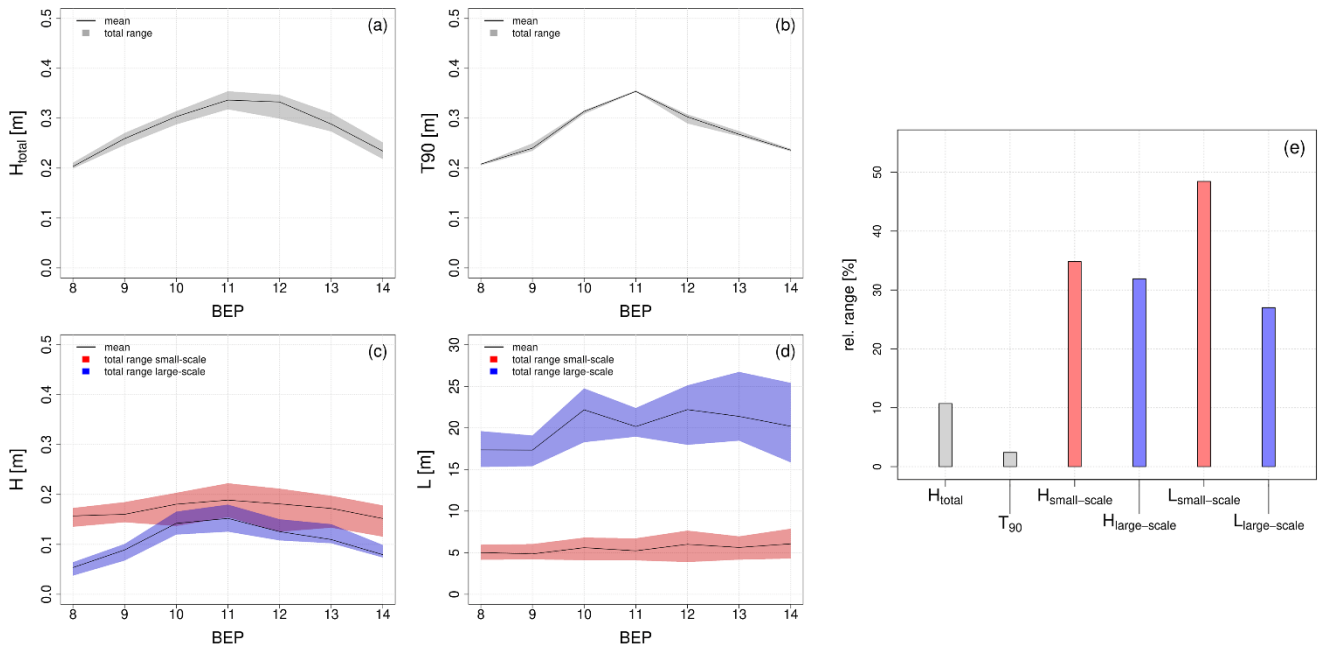
Figure 9: Resulting bedform parameters of the Monte Carlo Simulation. (a-d) - Identified ranges and mean values for individual BEPs. (e) – Averaged relative ranges over BEPs 8-14.

4.3 Bedform migration & bedload transport

To enable the calculation of bedform migration rates, repeated MBES-measurements were performed during the campaign, with a minimum time difference of 3.2 hours between two successive measurement for the entire bedform field. These intervals turned out to be too long, in order to track the faster migrating small-scale bedforms. Therefore, only the detailed measurements of the single measurement swath in the center (no. 5-14 in Table 3) are considered for the analysis of migration rates. Here, intervals are much shorter and start from 0.2 h. Based on the 10 available measurements, 45 pairwise combinations can be analyzed (see Appendix A, Table A1). Migration rates were calculated using two different methods as introduced in section 2.5.

Figure 10 shows the correlation coefficients derived from the cross-correlation analysis (method 1) as a function of time difference dt between two measurements. Correlation coefficients are shown here for the total BEP (without considering separate layers of bedforms) as well as for the individual layers. For considering the individual layers the constructed baselines from the MCS were used. Accordingly, for each measurement results from 100 iterations are available. For the total BEP, on the other hand, only one result per measurement is available. Correlation coefficients obviously decrease with increasing dt due to the deformation of bedforms. However, correlation coefficients of the large-scale bedforms and of the total BEP remain above a value of 0.7 even after 20 hours. Concerning the small-scale bedforms correlation coefficients decrease much more

 rapidly and drop below a value of 0.5 after less than two hours, highlighting that longer time differences between measurements are unsuitable for tracking these bedforms.
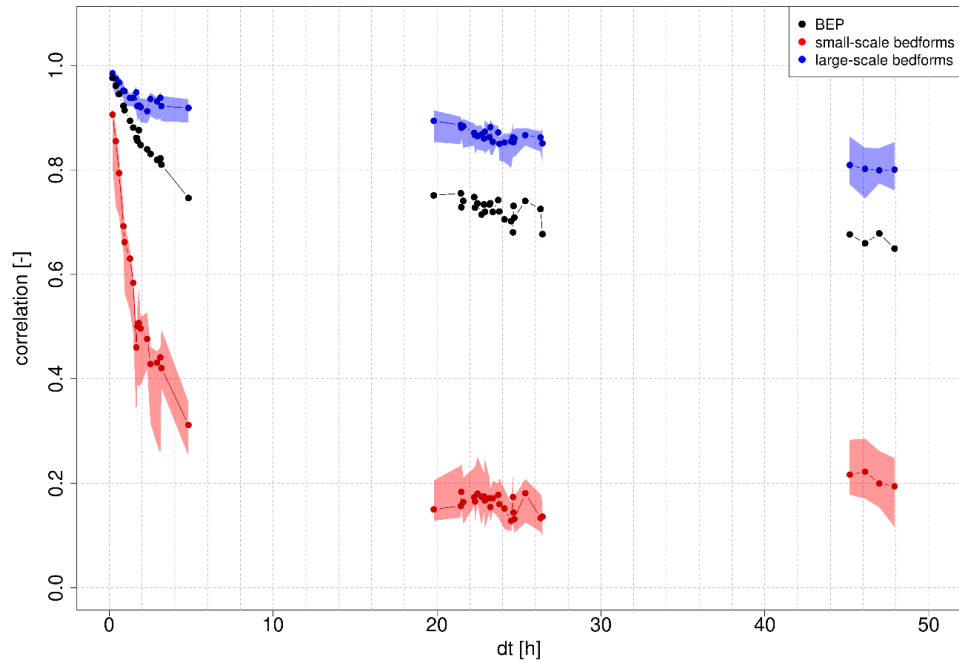
Figure 10: Correlations coefficients from the cross-correlation analysis (method 1) as a function of time difference between successive measurements. The red and blue dots represent the median values for small-scale and large-scale bedforms obtained
430 **from MCS. Polygons show the total range of results. For the total BEP only one results per measurement is available.**

By using method 2 (centroid analysis), migration rates for individual bedforms are determined. Individual migration rates are then filtered by the defined quality criteria considering the geometrical similarity of corresponding bedforms from two measurements. Figure 11 shows the remaining number of traceable bedforms. For the small-scale bedforms, the number of traceable bedforms strongly decreases as dt increases. For this reason, the results for longer measurement intervals should be
435 assessed with particular caution, as they are influenced by only a few observations. In contrast, the number of traceable large-scale bedforms is low for all measurement pairs and does not change significantly as dt increases, which is why we do not recommend to use this method to track underlying large-scale bedforms (see discussion section).
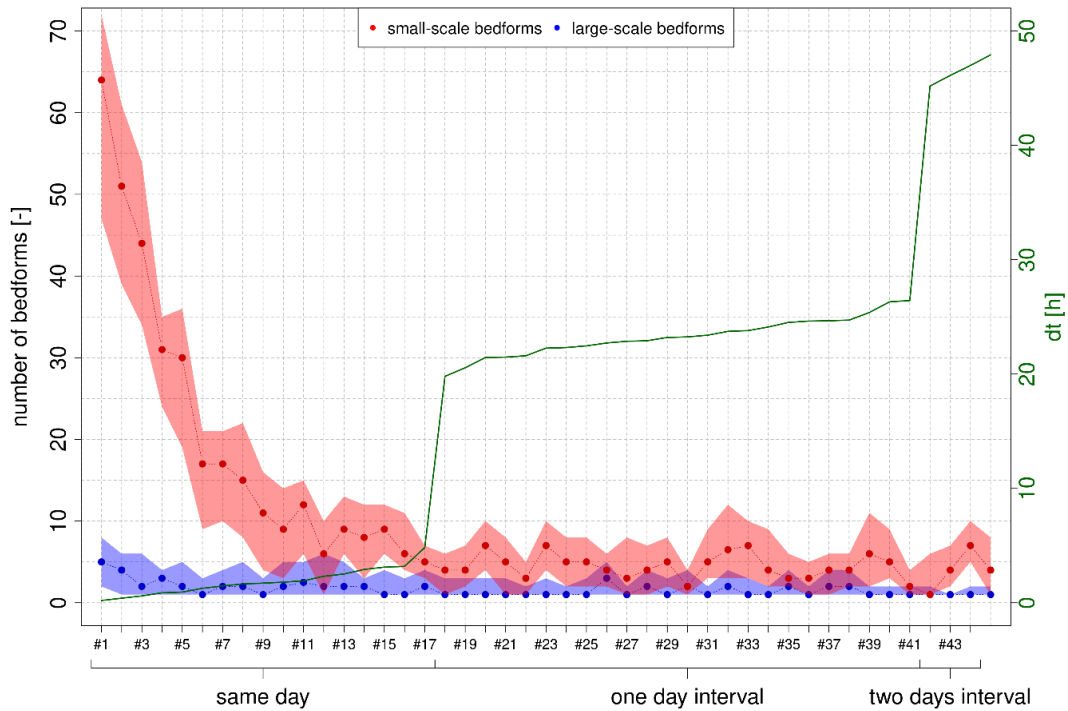
Figure 11: Number of traceable bedforms depending on measurement interval (centroid analysis, method 2). The red and blue dots
440 **represent the median values for small-scale and large-scale bedforms obtained from MCS. Polygons show the total range of results.**

Figure 12 summarizes determined migration rates for all 45 possible combinations of measurements for both methods. For

method 1 (cross-correlation analysis), results with correlation coefficients smaller than 0.5 were excluded. For method 2

(centroid analysis), after filtering the results, outliers exceeding a 95 % percentile were removed and then weighted average

445 migration rates were calculated along the BEP.

For method 1 median migration rates of the small-scale bedforms fluctuate between 1.5 and 2.2 m h^{-1}. For all measurement

pairs with a time difference of 2.5 h or more (above pair #12), the correlation coefficients drop below the 0.5 threshold value,

thus no reliable results are available. For the large-scale bedforms, median migration rates fluctuate between 0.1 and 0.8 m h^{-}

^{1}. For measurement pairs with a time interval of one day or more fluctuations are much lower. Concerning migration rates of

450 the total BEPs (without considering individual layers of bedforms), results for short measurement intervals are close to the

migration rates of the small-scale bedforms, while results for longer measurement intervals are close to the migration rates of

the large-scale bedforms, depending on which process is dominant. This highlights the need for considering individual bedform

layers in order to make precise statements about migration rates. Both, migration rates for the small-scale bedforms as well as

for the BEP decrease with increasing measurement intervals. This effect can probably be attributed to the fact that small

455 bedforms tend to migrate faster, but at the same time can only be reliably tracked for very short measurement intervals. For

small dt, the migration of small bedforms has a significant effect on the cross-correlation analysis (and thus on the determination of the best fitting spatial offset). With increasing dt, deformation of bedforms increases so that the smallest bedforms are no longer traceable and the average migration rate decreases (see also section 5.1.2). This effect can be found in the results of both methods.

460   Regarding method 2 (Figure 12b), fluctuations are higher compared to method 1. For the small-scale bedforms median migration rates vary between 1 m h^{-1} and 2 m h^{-1} for most of the measurement pairs that contain measurements of the same day. For longer measurement intervals (one day or two days interval) values vary between 0 m h^{-1} and 0.5 m h^{-1}. As shown in in Figure 11 the number of traceable bedforms drastically decreases with increasing dt, which is why only the results for very short measurement intervals are sufficiently reliable. Here, the results are quite comparable to those of method 1. Again,

465   migration rates decrease with increasing dt. The number of traceable large-scale bedforms is constantly low ($\leq$ 5). For short measurement intervals fluctuations are very high. For longer measurement intervals, however, migration median rates are again comparable to those obtained from method 1 and vary from 0.1 to 0.6 m h^{-1}.
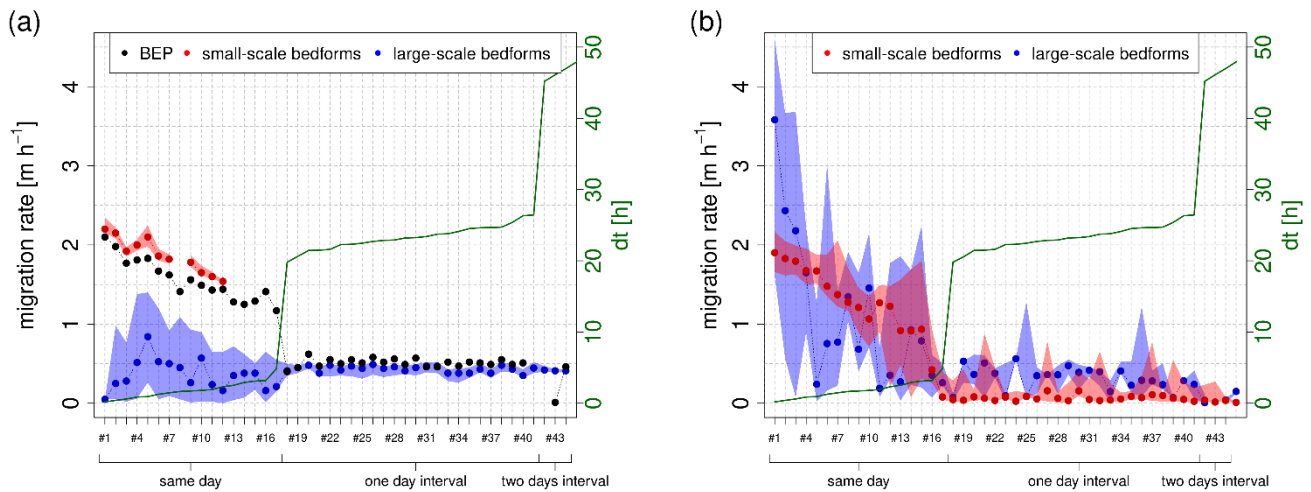
470   **Figure 12: Calculated migration rates for all respected measurement pairs by means of cross-correlation analysis (method 1, a) and centroid analysis (method 2, b).**

Based on the migration rates calculated by the two methods, bedload transport rates were estimated using Eq (4). As just

475   shown, the time difference between two measurements has a strong impact on resulting migration rates. The small-scale bedforms can only be tracked accurately by using short measurement intervals while longer intervals are more suitable for the large-scale bedforms. For this reason, only measurement intervals shorter than two hours were considered for the estimation of bedload transport due to the scmall-scale bedforms, whereas only measurement intervals longer than 19 hours (measurements carried out on different days) were considered for the large-scale bedforms. For estimating the total transport,

480 the quantities derived from both bedform layers were summed up. Figure 13 shows estimated bedload transport rates and their ranges resulting from the different input parameter settings within the MCS for both methods. Again, the results obtained from the centroid analysis are more affected leading to total bedload transport rates fluctuating within a range of about 60 g s^{-1} m^{-1} (corresponding to more than 50 % in relation to the median). In comparison those obtained from the cross-correlation analysis only fluctuate within a range of about 40 g s^{-1} m^{-1} (corresponding to about 30 % in relation to the median). Median values,

485 however, are in the same order of magnitude for both methods. Further on, both methods indicate that bedload transport associated with the small-scale bedforms accounts for nearly 90 % of the total transport, while bedload transport associated with the large-scale bedforms accounts for only slightly more than 10 %.
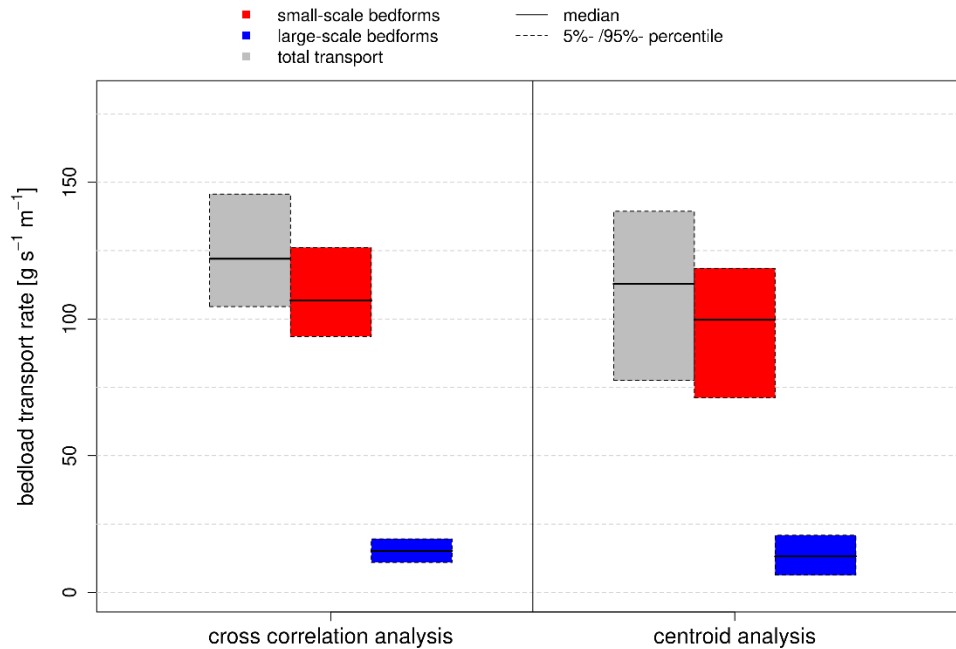
Figure 13: Comparison of bedload transport rates derived from cross-correlation and centroid analysis along the evaluated BEP.

490

5 Discussion

5.1 Interpretation of the results

5.1.1 Bedform geometries

The results for bedform geometries (refer to section 4.2) show lowest uncertainties for the bedform parameters, that measure

495 the total height. Here, we determined values of 2 % for T_{90} and 10 % for H_{total}. The heights of the individual layers, on the

other hand, show significantly higher uncertainties of 30 to 35 %. The greatest uncertainties arise in the determination of bedform lengths, which reach values of up to 50 %. We recognized that uncertainties in the determination of bedform geometries are lower if the geometries of the individual layers are considered together as composite entities. In this case, the calculated attributes only depend on the baseline of the large-scale bedforms, which separates the bedforms from the underlying
500 non-active layer of the river bed. They are independent of the baseline of small-scale bedforms which separates both layers from each other. At the same time, we show in section 5.2 that the *window size* for the small-scale bedforms is the most sensitive input parameter. This explains why determined uncertainties are lower for total heights compared to heights of the individual layers.

Furthermore, bedform lengths were subject to higher uncertainties than bedform heights, especially for the small-scale
505 bedforms. The specific morphological situation for the test dataset from Lower Rhine could have had an influence on this result. It is noticeable that the analyzed bedforms of both layers are rather similar in height and differ mainly in their length (see Figure 9c/d). For most BEPs both layers have average heights of approx. 10 cm to 20 cm, while the average lengths are approx. 5 m to 6 m and 17 m to 22 m respectively. There are other cases where both length and height differ by an order of magnitude, as e.g. in datasets from the Rio Paraná as published in Parsons et al. (2005) or from the river Waal as published in
510 Zomer et al. (2023). The analysis should therefore be continued by using datasets with different morphological conditions in order to validate this finding.

The measurements from Lower Rhine were carried out a few days after a peak in discharge. Findings from other studies indicate that significant changes in bedform characteristics may occur during the falling flood limb, which are very much in line with our observations for the dataset from Lower Rhine. According to Martin and Jerolmack (2013) the larger primary
515 bedforms become inactive during the fall of the flood and are cannibalized by the formation of smaller bedforms, in equilibrium with the decreased discharge. In the study of Wilbers and Ten Brinke (2003), smaller secondary bedforms were observed emerging during the falling flood limb while shrinking heights and increasing lengths were observed for primary bedforms. In Zomer et al. (2023), however, secondary bedforms were observed over the full range of flow conditions. To demonstrate that we found similar conditions for the dataset from Lower Rhine, the height to length ratio of detected bedforms is plotted in
520 comparison to the maximum and mean bedform height according to Flemming (1988) in Figure 14. While the small-scale bedforms fit in quite well with Flemming's ratio, the large-scale bedforms are less steep and are shifted accordingly to the right. Corresponding to the observations of the aforementioned studies, the emergence and migration of small-scale bedforms could have resulted in shrinking heights (and retarded migration) of the large-scale bedforms after the peak in discharge (this would also explain the high contribution of the small-scale bedforms to the total bedload transport). However, no further
525 measurement data are available to confirm this conclusively, as investigating the temporal development of bedforms during a flood wave was no initial objective of this study.
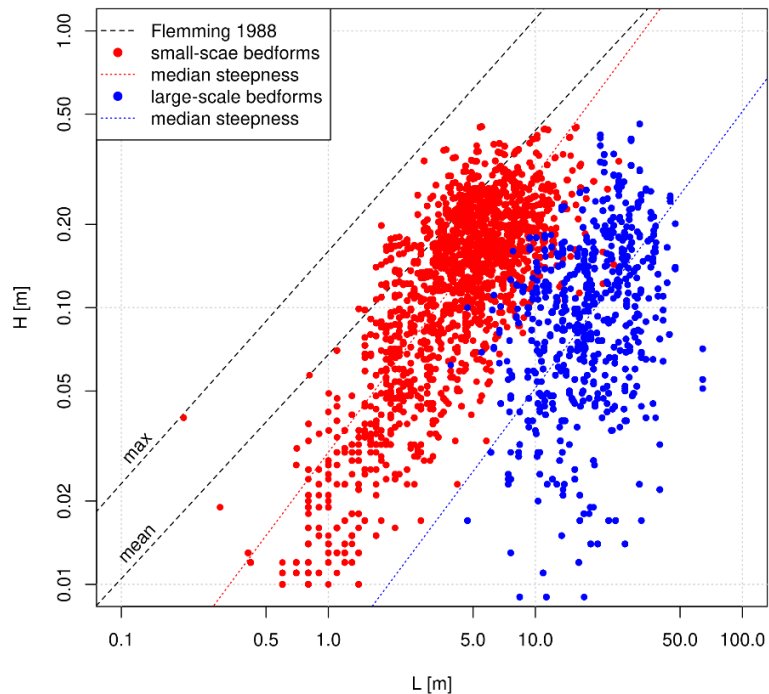
Figure 14: Ratio of identified bedform heights and lengths obtained from MBES-data from Lower Rhine (February 2020) compared to mean and maximum bedform height according to Flemming (1988).

530   The performed MCS revealed high uncertainties in the determination of bedform geometries, which resulted from different input parameter settings. However, there are other sources of uncertainty in the determination of bedform geometry like the choice of method or tool in general. For example, in the recently published meta-analysis by Scheiber et al. (2024) five bedform identification algorithms were compared. They were divided into two groups based on methodological similarities. Within each group deviations in median heights and lengths did not exceed a value of 25 % after efforts were made to standardize

535   inputs (e.g. harmonizing definitions of bedform attributes). Between the two groups much higher deviations were found. Another source of uncertainty is described by Scheiber & Lefebvre (2022). They show that the definition of bedform height (there are various possible and common ways to geometrically determine the height of an individual bedform) can have an even higher influence on the resulting values. Here, relative differences of over 100 % were identified. Further on, the influence of data preprocessing like the generation of DEMs and BEPs could also be considered. By collating all this information about

540   the multiple sources of uncertainty, the picture can be gradually completed.

5.1.2 Bedform migration & bedload transport

In section 4.3 we showed the results for bedform migration that were derived from the MCS by using the multiple solutions obtained from the zerocrossing procedure. We investigated how the influence of the different input parameter settings for the zerocrossing procedure propagates to the determination of bedform dynamics. In addition, the influence of the measurement

545 interval was evaluated. These results reveal that the determined migration rates as well as their uncertainties depend on the time difference between two measurements. This time difference determines the highest possible traceable migration rate and thus, at the same time, the minimum bedform dimensions that can be considered (since it is assumed that migration rates increase with decreasing bedform dimensions). Even within an individual layer, there is heterogeneity in terms of bedform dimensions. The smaller the time difference, the smaller the bedforms that can be tracked accurately. An increase in time

550 difference leads to an increasing loss of information and eventually to a potential underestimation of bedform migration and bedload transport rates, since the faster migrating smaller bedforms are no longer identified. In the centroid analysis these are successively removed from the analysis as they no longer meet the defined quality criteria. In the cross-correlation analysis the influence of larger bedforms within an individual layer increases with increasing time difference. This explains the decreasing trend in Figure 12 regarding migration rate of the small-scale bedforms, which was found by using both methods.

555 Exceeding a measurement interval of two hours, migration of small-scale bedforms can no longer be tracked, which eventually leads to an underestimation of bedform migration and bedload transport (it was shown that the migration of small-scale bedforms accounted for about 90 % of the total bedload transport!). On the other hand, in order to track the underlying large-scale bedforms, longer measurement intervals appeared to be more suitable as they are subject to significantly lower scattering. For short intervals (measurements carried out on the same day) deviations of more than 100 % were reached in cross-correlation

560 analysis (Figure 12a). This underlines that in order to track both small- and large-scale bedforms accurately, different intervals and therefore multiple measurements are required. It could be helpful to perform preliminary measurements to get a first impression about prevailing bedform dimensions and migration rates and to select suitable intervals based on this.

In this study, a second method was used for determining bedform dynamics. The newly introduced centroid analysis appeared to be subject to greater uncertainties, especially regarding migration of large-scale bedforms. As shown in Figure 11 the number

565 of traceable bedforms is constantly low for the large-scale bedforms. We therefore recommend not to use this new method to track underlying large-scale bedforms, since for short measurement intervals the spatial offset is too small to enable a precise assignment (approaching the limit in terms of measurement accuracy) whereas for large intervals deformation already has too much influence on the calculation of the geometric centroids. However, another reason for the smaller number of traceable large-scale bedforms can be found in the distribution of larger bedforms along the BEPs. While small-scale bedforms can be

570 found along the entire BEP, large-scale bedforms are only present in certain subsections and are not covering the total length of the BEP. The added value of the new method is a deeper look at the behavior of individual bedforms – in relation to their geometric attributes – as well as information on the longitudinal variability of bedload transport. From this, new insights can be gained especially concerning the behavior of rapidly migrating smaller bedforms, which can end up contributing the largest part to the total bedload transport.

575 As mentioned above there are multiple sources of uncertainty in the determination of bedform geometries. When deriving bedload transport rates from these, others are added like the uncertainty in the estimation of porosity and grain density or even the uncertainty in choosing an empirical formula for the calculation. Again, these sources of uncertainty must be added, in order to complete this consideration.

A more detailed look at the performance of different bedload transport measurement techniques and – among other aspects -
580 at possible factors influencing the dunetracking method were the subject of the so-called LILAR-campaign (BfG, 2023). The campaign was carried out in November 2021 as cooperation of German and Dutch authorities. One of the objectives was to compile, compare and evaluate different methods for measuring sediment transport. In addition, we are planning to perform further campaigns to investigate the influence of different discharge conditions on bedform characteristics in more detail. For this kind of comparative studies, it is again essential to estimate the uncertainties in bedform analysis, in order to robustly
585 evaluate occurring changes.

5.2 Sensitivity of the input parameters

In section 5.1 we discussed the influence of input parameter settings on the calculated of bedform characteristics and bedload transport rates. In this section, we discuss which of the input parameters has the greatest influence. A sensitivity analysis was performed, in which only one input parameter was varied at a time while the others were kept constant. Table 4 shows the
590 three chosen input parameter settings. For the parameters that were kept constant, a mean value was set based on the results from the wavelet analysis (see Figure 8).

Table 4: Input parameter for sensitivity analyses.

setting	window size small-scale bedforms [m]	window size large-scale bedforms [m]	zc-threshold [cm]
1	1 – 20	25	0.5
2	8	20 – 30	0.5
3	8	25	0.5 – 5

595 **5.2.1 Bedform geometries**

Figure 15 shows the potential influence of the input parameters *window size* for small- (a-c) and large-scale bedforms (d-f) as well as *zc-threshold* (g-i) on the resulting bedform geometries (T90, H_{total} $L_{1,2/total}$). The resulting bedform geometries were averaged over the considered BEPs no. 8-14. Increasing the *window size* for the small-scale bedforms (setting 1) results in increasing bedform heights and lengths. The parameter is especially sensitive during the first iterations. When exceeding a
600 value of about five meters, increasing convergence can be observed for both bedform heights and lengths. Within the selected range of *window sizes* based on the wavelet analysis (grey area), only a very low variability can be observed. So, the sensitivity is particularly high outside this selected range. Overall, with respect to bedform height the T90-parameter behaves less sensitive than the H_{total}-parameter. The reason for this is that the T90-parameter is independent of the number of identified bedforms. It

is not based on measuring individual bedform heights but on measuring the accumulated bedforms layer thickness (T) in every

605   x-position along the entire BEP. So, always the same number of input values is used for the calculation.

The *window size* for the large-scale bedforms (setting 2) has almost no influence on the T90-parameter (Figure 15d). With respect to the H_{total}-parameter, a very slight increase (2 cm) can be observed with increasing *window size* (Figure 15e). Bedform length (in this case only the large-scale bedforms are affected), again, exhibits more sensitivity. Here, no convergence can be

610   observed (Figure 15f). Nevertheless, variability is much smaller compared to setting 1. It can be assumed that convergence will eventually occur with increasing values, as the calculated moving average value successively approaches a horizontal line. The influence of the *zc-threshold* (setting 3) is also much smaller than that of the *window size* for the small-scale bedforms. Bedform heights exhibit less sensitivity than bedform lengths, for which no convergence occurs (Figure 15i). By increasing the *zc-threshold,* local minima are filtered out successively (see Sect. 2). Thereby, several individual bedforms are summarized,

615   resulting in a smaller number of longer bedforms. While the maximum height is limited by the lowest and the highest point in a BEP, a successive increase in length - by combining several individual bedforms - is technically possible. This is why it is important to consider the expected bedform dimensions, in order not to obtain implausible results.
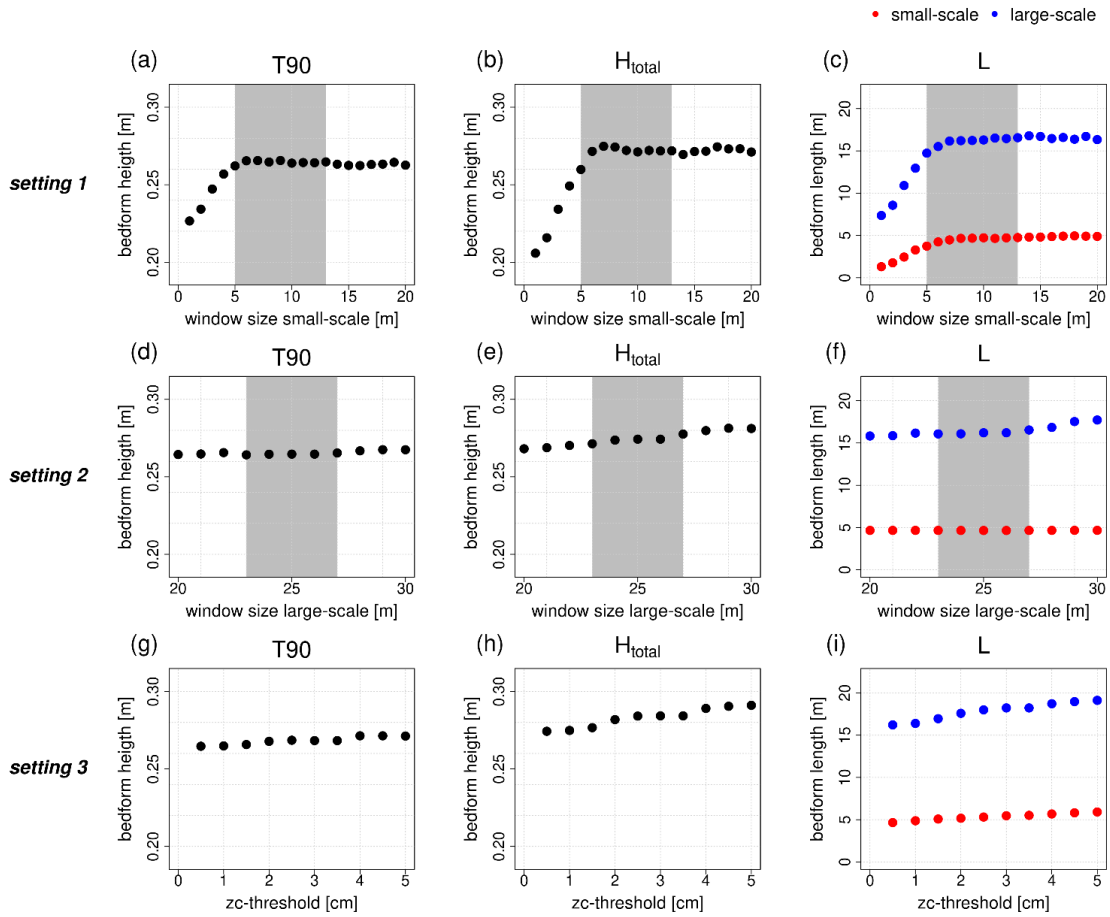
620 **Figure 15: Influence of variation in the input parameters on derived bedform geometries (grey area corresponds to the selected value range based on the wavelet analysis).**

Changing *window size* for the small-scale has the strongest impact on resulting bedform geometries. Concerning bedform height, the T90-parameter appears to be more robust towards varying input parameter settings compared to the H_{total}-parameter.
625 Overall, bedform lengths appear to be more sensitive and include a higher degree of uncertainty. While the H_{total}-parameter shows a maximum variability of about 30 %, the total length (corresponding to the length of the large-scale bedforms) shows a maximum variability about 60 %. (both for setting 1). The delineation of two adjacent bedforms is not always obvious and several different solutions might be conceivable. Even a manual delineation is a highly subjective process and could lead to different solutions for different investigators. For many cases a convergence pattern can be observed, that starts at the lower
630 margin of *window sizes* based on the results from the wavelet analysis (grey shaded area in Figure 15). *Window sizes* smaller than the lower margin, lead to diverging results, which confirms the need for performing the wavelet analysis as an orientation. These findings should be taken into account when analyzing bedform geometries, such as studies on the relationship between bedform height and length (e.g. Flemming 1988; Lefebvre et al. 2022). Individual bedform attributes are often displayed in

scatterplots. According to the findings of this study, an uncertainty range would have to be specified for each data point in a
635   scatterplot, based on different input parameter settings in the evaluation procedure. So, we would recommend to investigate
the sensitivity of input parameter for other methods as well. The shown results provide an indication of the possible order of
magnitude.

5.2.2 Bedform migration & bedload transport

Figure 16 shows the results of the sensitivity analysis for the calculation of bedform migration and bedload transport rates
640   based on the cross-correlation analysis (method 1). For this purpose, the resulting parameters were averaged over different
measurement intervals. Based on the findings presented in section 4.3, only measurement intervals shorter than two hours were
considered for the small-scale bedforms whereas only measurement intervals longer 19 hours (measurements carried out on
different days) were considered for the large-scale bedforms.

Increasing *window sizes* for the small-scale bedforms lead to decreasing bedform migration rates that converge to a value of
645   about 2 m s^{-1} for *window sizes* > 5m (Figure 16a). For smaller *window sizes* smaller bedforms are derived from the BEPs,
which are migrating with higher rates. At the same time, bedload transport rates for the small-scale bedforms increase with
increasing *window size* as bedform area increases, which overweighs the influence of decreasing migration rates. They
converge to a value of about 110 g s^{-1} m^{-1} (Figure 16b). Bedform area for the large-scale bedforms, however, decreases with
increasing bedform area for the small-scale bedforms due to a different delineation of the total geometry. As a result, bedload
650   transport rates for the large-scale bedforms decrease as well. Correlation coefficients increase with increasing *window size* for
the small-scale bedforms (Figure 16c). This is because small bedforms resulting from small *window sizes* can only be traced
accurately for very short measurement intervals. So, averaged correlation coefficients are lower for smaller window sizes. The
large-scale bedforms are only slightly affected. Overall, highest variability can be found outside the chosen range of *window
sizes* for the small-scale bedforms based on the wavelet analysis.

655   Varying *window sizes* for the large-scale bedforms do not have any influence on the cross-correlation analysis. This is because
the baselines of the large-scale bedforms are not included in the analysis (see section 2.5). Only the changing (increasing)
bedform areas result in a slight increase in bedload transport rates for the large-scale bedforms (Figure 16e).

Concerning the behavior of the *zc-threshold*, similar effects can be observed as for the *window size* for the small-scale bedforms
at setting 1, however, they turn out to be significantly less sensitive (Figure 16g-i). Correlation coefficients stay rather constant
660   over all iterations (Figure 16i).
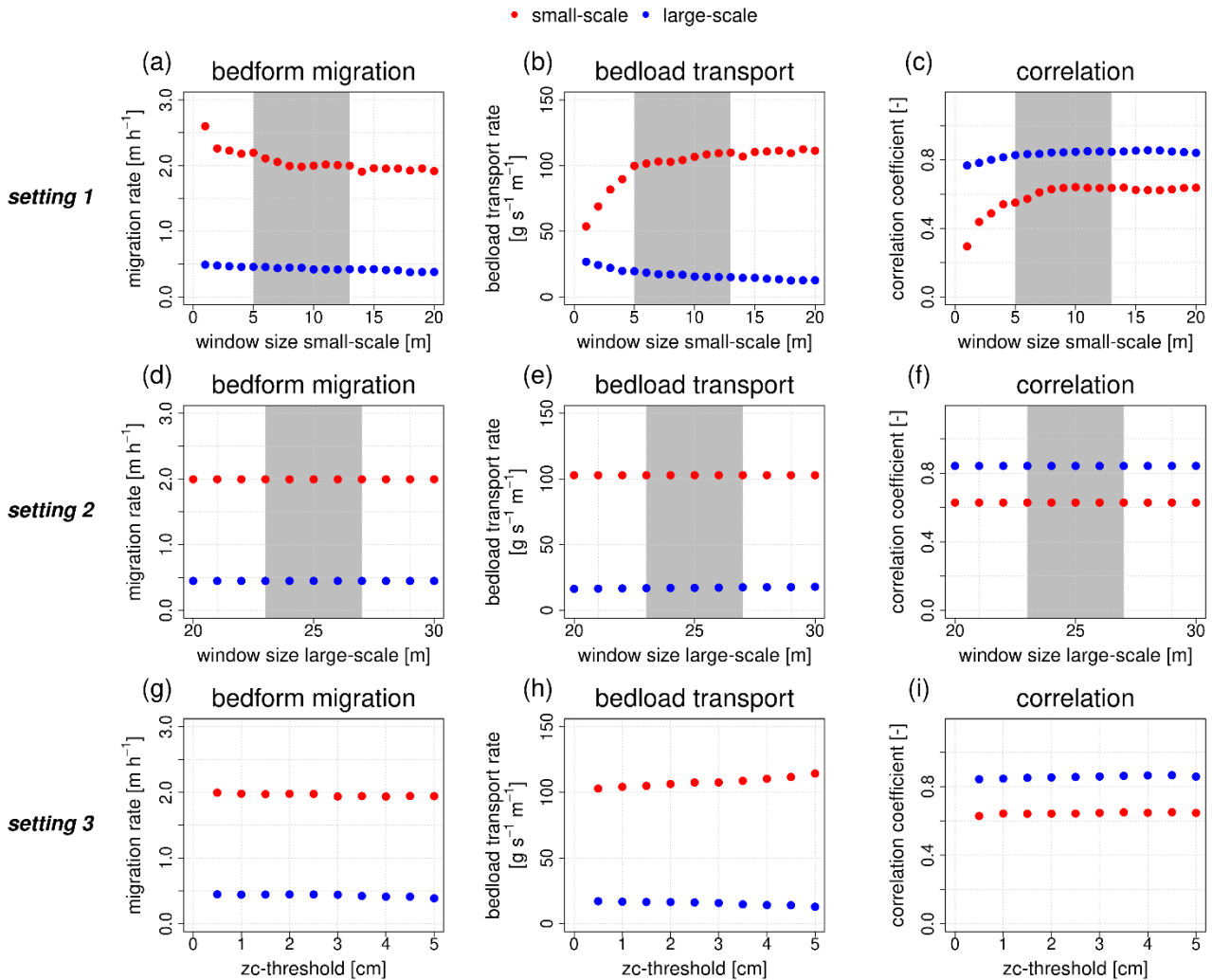
Figure 16: Influence of variation in the input parameters on the cross-correlation analysis (grey area corresponds to the selected value range based on the wavelet analysis).

Figure 17 shows the influence of input parameter settings on the centroid analysis (method 2). As explained in the previous sections the method is rather suitable for small-scale bedforms and short measurement intervals. This is why the small-scale bedforms and only those measurement pairs with intervals shorter than two hours are considered here (see section 4.3).

At setting 1, migration rates initially increase with increasing *window size* (Figure 17a). A maximum is reached at a value of 3 m. A further increase in *window size* leads to decreasing migration rates with a tendency to convergence to a value of 1.5 m s^{-1}. Bedload transport rates first increase and then tend towards a value of 100 g s^{-1} m^{-1} (Figure 17b). Very small bedforms can only be traced accurately at very short measurement intervals, so that a rapid increase in the number of detected bedforms can be observed with increasing *window size* (Figure 17c). After reaching a maximum at a value of 10 m the number of traceable

bedforms decreases again. An increasing *window size* leads to increasing bedform areas and thus to a decreasing number of bedforms. Again, for all parameters highest variations are found outside the chosen range of *window sizes*.

675 Varying the setting of the *zc-threshold* again has much less impact on the results. No systematic effect on the centroid analysis can be observed (Figure 17d-e).
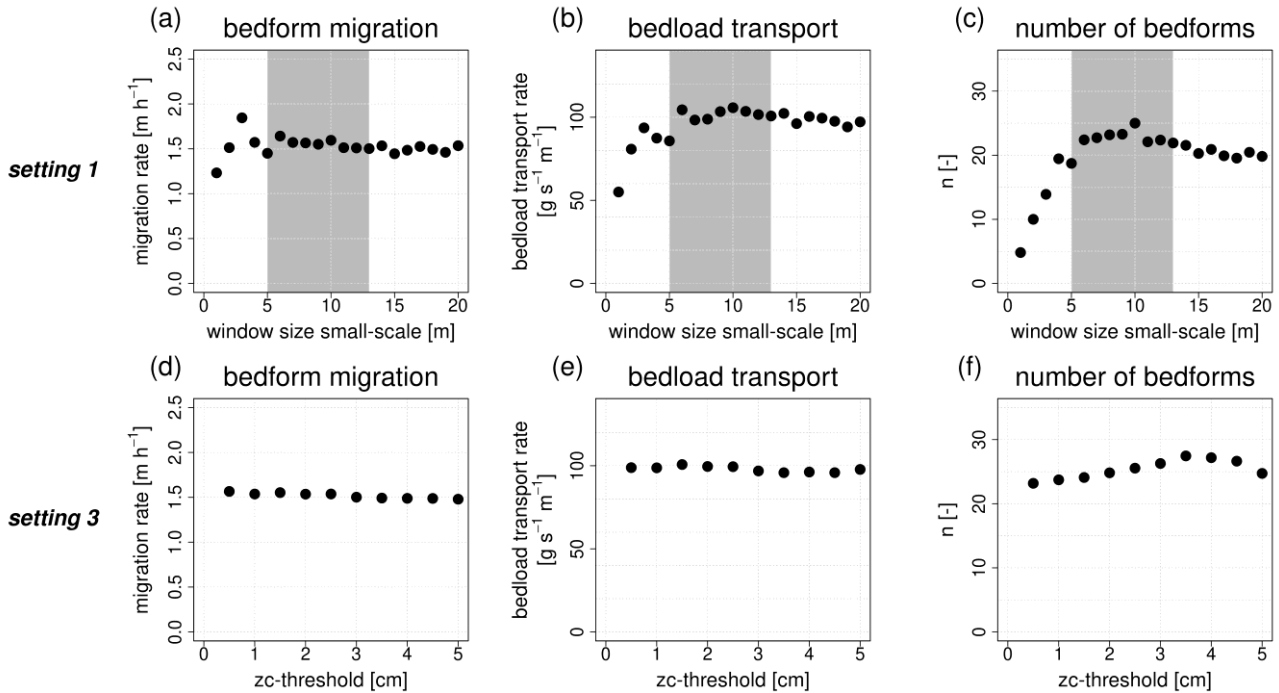
Figure 17: Influence of variation in the input parameters on the centroid analysis (grey area corresponds to the selected value range based on the wavelet analysis).

680 As for bedform geometries, it can also be observed for bedform migration and bedload transport that setting 1 has the greatest influence on the resulting parameters. This is true for both methods. Again, outside the chosen range of *window sizes* based on the results from the wavelet analysis, increasing divergence can be seen. The results illustrate that the effect of varying input parameter settings in the zerocrossing procedure propagates to the determination of bedform dynamics.

Conclusions

685 Bedform analysis tools are sensitive to the influence of input parameters. Often, no theoretically sound criteria are available for the setting of input parameters with specific values. So, this decision depends on the subjective assessment of the investigator. Therefore, we developed a highly automated workflow, which allows the quantification of uncertainties in the calculation of bedform parameters due to different input parameter settings by an MCS-routine. We implemented different methods to analyze both, bedform geometry and dynamics. In terms of bedform geometry, we combined a wavelet analysis

690 based on Bedforms-ATM (Gutierrez et al., 2018) with the well-established and widely used zerocrossing-procedure. In terms

of bedform dynamics we implemented a cross-correlation analysis as well as the newly introduced centroid analysis. By applying this workflow to a test dataset from Lower Rhine in Germany, the following main results and key conclusions can be derived.

- Bedform parameters react with different sensitivity to varying input parameter settings. Lowest uncertainties were found when individual layers of bedforms were considered together as composite entities without discriminating between them. Especially the introduced T90-parameter, as a measure of total bedform height, proved to be very robust with uncertainties of only 2 %. Uncertainties for the heights of individual bedform layers, on the other hand, appeared to be much higher between 30 % and 35 %. Highest uncertainties were identified for bedform lengths reaching values of up to 50 % for the small-scale bedforms. Uncertainties regarding bedform geometries are propagated to the determination of bedform migration and bedload transport rates.

- Uncertainties for bedload transport rates were found in the order of 30 % (by using the cross-correlation analysis) to 50 % (by using the centroid analysis). By applying both methods it could be shown that the migration of the small-scale bedforms accounted for about 90 % of the total bedload transport.

- Regarding bedform dynamics there also is an uncertainty due to varying time differences between two consecutive measurements. Rapidly migrating secondary bedforms were only traceable for measurements with time differences of less than two hours. For those measurements a decrease in migration rate was observed for increasing time difference. On the other hand, for tracking the underlying large-scale bedforms using longer measurement intervals resulted in lower uncertainties. We therefore recommend choosing measurement intervals with care and depending on the process under investigation. Performing preliminary measurements to get a first impression about prevailing conditions may support this decision.

- With regard to the question of which input parameter has the greatest influence on the resulting bedform parameters, the *window size* for the small-scale bedforms was identified as the most sensitive. Especially for very small values, an increase *in window size* has a significant impact on bedform geometries as well as on bedform migration and bedload transport rates.

- The most stable results were found inside the range of values provided by the wavelet analysis (based on Bedforms-ATM) in the first step of the workflow. This underlines the importance of performing the wavelet analysis to narrow the range of values entering the MCS. It was shown that values below the specified range strongly influence the results and lead to divergence.

- Overall, it was shown that varying input parameter settings can have a large influence on the determination of bedform parameters. But at the same time, we have introduced a workflow that can provide proof of robust estimates of these parameters. We therefore recommend carrying out similar investigations for other bedform analysis methods and datasets, in order to assess the robustness of derived results. However, in this study we focused on the uncertainties resulting from varying input parameter settings. There are multiple sources of uncertainties in bedform analysis like

725   the choice of a method or tool in general or the geometric definitions of bedform attributes. All these uncertainties must be considered together in field studies characterizing prevailing bedform conditions derived from measurement data.

Appendices

Appendix A

730   **Table A1: 45 evaluated measurement pairs obtained from detail measurements.**

no.	date 1	time 1 (MET)	date 2	time 2 (MET)	Δt [h]
1	18 February 2020	10:29	18 February 2020	10:41	0.2
2	18 February 2020	10:41	18 February 2020	11:05	0.4
3	18 February 2020	10:29	18 February 2020	11:05	0.6
4	18 February 2020	11:05	18 February 2020	11:57	0.9
5	17 February 2020	11:17	17 February 2020	12:13	0.9
6	18 February 2020	10:41	18 February 2020	11:57	1.3
7	18 February 2020	10:29	18 February 2020	11:57	1.5
8	18 February 2020	11:57	18 February 2020	13:36	1.6
9	18 February 2020	8:46	18 February 2020	10:29	1.7
10	19 February 2020	9:24	19 February 2020	11:12	1.8
11	18 February 2020	8:46	18 February 2020	10:41	1.9
12	18 February 2020	8:46	18 February 2020	11:05	2.3
13	18 February 2020	11:05	18 February 2020	13:36	2.5
14	18 February 2020	10:41	18 February 2020	13:36	2.9
15	18 February 2020	10:29	18 February 2020	13:36	3.1
16	18 February 2020	8:46	18 February 2020	11:57	3.2
17	18 February 2020	8:46	18 February 2020	13:36	4.8
18	18 February 2020	13:36	19 February 2020	9:24	19.8
19	17 February 2020	12:13	18 February 2020	8:46	20.6
20	18 February 2020	11:57	19 February 2020	9:24	21.4
21	17 February 2020	11:17	18 February 2020	8:46	21.5

22	18 February 2020	13:36	19 February 2020	11:12	21.6
23	17 February 2020	12:13	18 February 2020	10:29	22.3
24	18 February 2020	11:05	19 February 2020	9:24	22.3
25	17 February 2020	12:13	18 February 2020	10:41	22.5
26	18 February 2020	10:41	19 February 2020	9:24	22.7
27	17 February 2020	12:13	18 February 2020	11:05	22.9
28	18 February 2020	10:29	19 February 2020	9:24	22.9
29	17 February 2020	11:17	18 February 2020	10:29	23.2
30	18 February 2020	11:57	19 February 2020	11:12	23.2
31	17 February 2020	11:17	18 February 2020	10:41	23.4
32	17 February 2020	12:13	18 February 2020	11:57	23.7
33	17 February 2020	11:17	18 February 2020	11:05	23.8
34	18 February 2020	11:05	19 February 2020	11:12	24.1
35	18 February 2020	10:41	19 February 2020	11:12	24.5
36	18 February 2020	8:46	19 February 2020	9:24	24.6
37	17 February 2020	11:17	18 February 2020	11:57	24.7
38	18 February 2020	10:29	19 February 2020	11:12	24.7
39	17 February 2020	12:13	18 February 2020	13:36	25.4
40	17 February 2020	11:17	18 February 2020	13:36	26.3
41	18 February 2020	8:46	19 February 2020	11:12	26.4
42	17 February 2020	12:13	19 February 2020	9:24	45.2
43	17 February 2020	11:17	19 February 2020	9:24	46.1
44	17 February 2020	12:13	19 February 2020	11:12	47
45	17 February 2020	11:17	19 February 2020	11:12	47.9

Code & data availability

The introduced tool (code and test dataset) is accessible via: https://github.com/JRbfg/DTMCS

Author contribution

JR developed the code, performed all analyses and prepared the paper with the cooperation of AW. AW provided support regarding the technical discussion of the results as well as regarding the composition of the paper.

Competing interests

The contact author has declared that none of the authors has any competing interests.

Acknowledgements

The measurements to collect test dataset used in this paper were performed by the Federal Waterways and Shipping Administration (Wasserstraßen- und Schifffahrtsverwaltung des Bundes, WSV). The hydrographic processing and the provision of the individual BEPs were carried out by Felix Lorenz and Thomas Artz from the Federal Institute of Hydrology (Department for Geodesy and Remote Sensing). We are grateful for the provision of the data.

Funding

Large parts of this work were part of the MAhyD project (morphodynamic analyses using hydroacoustic data, Morphodynamische Analysen mittels hydroakustischer Daten – Sohlstrukturen und Geschiebetransport). The MAhyD project was funded by the Federal Ministry for Digital and Transport (BMDV).

References

Adekitan, A.I. (2014). Monte Carlo Simulation. 10.13140/RG.2.2.15207.16806.

BfG (2011). Sedimentologisch-Morphologische Untersuchung des Niederrheins. BfG 1768, 32.

BfG (2023). Living Lab Rhine (LILAR): Comparison of Sediment Measurement Methods Between the Netherlands and Germany. BfG 2141, Bundesanstalt für Gewässerkunde, Koblenz

Carling, P., Gölz, E., Orr, H., Radecki-Pawlik, A. (2000). The morphodynamics of fluvial sand dunes in the River Rhine, near Mainz, Germany. I. Sedimentology and morphology. Sedimentology. 47. 227 - 252. 10.1046/j.1365-3091.2000.00290.x.

Cisneros, J., Best, J., van Dijk, T., Almeida, R. P. D., Amsler, M., Boldt, J., et al. (2020). Dunes in the world's big rivers are characterized by low-angle lee-side slopes and a complex shape. Nature Geoscience, 13(2), 156–162. https://doi.org/10.1038/s41561-019-0511-7.

Claude, N., Rodrigues, S., Bustillo, V., Bréhéret, J., Macaire, J., Jugé, P. (2012). Estimating bedload transport in a large sand–gravel bed river from direct sampling, dune tracking and empirical formulas. Geomorphology. 179. 40–57. 10.1016/j.geomorph.2012.07.030.

Flemming, B. W. (1988). On the classification of subaquatic flow-transverse bedforms. Bochumer Geologische und Geotechnische Arbeiten, 29, 44–47. Retrieved from https://www.researchgate.net/profile/Burghard-Flemming/publication/271909932_On_the_classification_of_subaquatic_flow-transverse_bedforms/links/54d679a80cf2970e4e6dc399/On-the-classification-of-subaquatic-flow-transverse-bedforms.pdf

Frings, R.M., Gehres, N., de Jong, K., Beckhausen, C., Schüttrumpf, H. and Vollmer, S. (2012). Rheno BT, User Manual, Institute of Hydraulic Engineering and Water Resources Management, RWTH Aachen University.

Gilja, G., Kuspilić, N., Brckan, B. (2013). Computer algorithm for analysis of bedform geometry. Conference: 13th International Symposium on Water Management and Hydraulic Engineering

Gutierrez, R. R., Abad, J. D., Parsons, D. R., & Best, J. L. (2013). Discrimination of bed form scales using robust spline filters and wavelet transforms: Methods and application to synthetic signals and bed forms of the Río Paraná, Argentina. Journal of Geophysical Research: Earth Surface, 118(3), 1400– 1418. https://doi.org/10.1002/jgrf.20102

Gutierrez, R.R., Mallma, J.A., Núñez-González, F., Link, O. and Abad, J.D. (2018). Bedforms-ATM, an open source software to analyze the scale-based hierarchies and dimensionality of natural bed forms. SoftwareX, 7, pp.184-189.

Henning, M. (2013). Mehrdimensionale statistische Analyse räumlich und zeitlich hoch aufgelöster Oberflächen von Dünenfeldern. https://doi.org/10.24355/dbbs.084-201306140925-0.

Kleinhans, M. (2001). The key role of fluvial dunes in transport and deposition of sand–gravel mixtures, a preliminary note. Sedimentary Geology. 143. 7-13. 10.1016/S0037-0738(01)00109-9.

Kleinhans, M., Wilbers, A.W.E., Swaaf, A., Berg, J. (2002). Sediment Supply-Limited Bedforms in Sand-Gravel Bed Rivers. Journal of Sedimentary Research. 72. 10.1306/030702720629.

Leary, K. & Buscombe, D. (2020). Estimating sand bed load in rivers by tracking dunes: a comparison of methods based on bed elevation time series. Earth Surface Dynamics. 8. 161-172. 10.5194/esurf-8-161-2020.

Lebrec, U., Riera, R., Paumard, V., O'Leary, M. J., & Lang, S. C. (2022). Automatic mapping and characterisation of linear depositional bedforms: Theory and application using bathymetry from the North West Shelf of Australia. Remote Sensing, 14(2), 280. https://doi.org/10.3390/rs14020280.

Lee, J., Musa, M., & Guala, M. (2021). Scale-dependent bedform migration and deformation in the physical and spectral domains. Journal of Geophysical Research: Earth Surface, 126(5), e2020JF005811. https://doi.org/10.1029/2020JF005811.

Lefebvre, A. & Winter, C. (2016). Predicting bed form roughness: the influence of lee side angle. Geo-Marine Letters. 36. 10.1007/s00367-016-0436-8.

Lefebvre, A., Herrling, G., Becker, M., Zorndt, A., Krämer, K. & Winter, C. (2022). Morphology of estuarine bedforms, Weser Estuary, Germany. Earth Surface Processes and Landforms, 47(1), 242–256. Available from: https://doi.org/10.1002/esp.5243

Lorenz, F., Artz, T., Brüggemann, T., Reich, J., Weiß, R., Winterscheid, A. (2021a). Simulation-based Evaluation of Hydrographic Data Analysis for Dune Tracking on the River Rhine. PFG – Journal of Photogrammetry Remote Sensing and Geoinformation Science. 89. 1-10. 10.1007/s41064-021-00145-0.

Lorenz, F., Artz, T., Brüggemann, T., Reich, J., Weiß, R. and Winterscheid, A. (2021b) Simulation-based Measurement

795 Strategies for Dune Tracking with Multi Beam Echosounders. FIG e-Working Week 2021.

McElroy, B., Mohrig, D. (2009). Nature of deformation of sandy bed forms, J. Geophys. Res.-Earth, 114, F00A04, https://doi.org/10.1029/2008JF001220.

Martin, R. L. and Jerolmack, D. J. (2003): Origin of hysteresis in bed form response to unsteady flows, Water Resour. Res., 49, 1314–1333.

800 Nyander, A., Addison, P.S., McEwan, I., Pender, G. (2003). Analysis of river bed

surface roughnesses using 2D wavelet transform-based methods. The Arabian Journal

for Science and Engineering, 28(1C):107-121.

Ogor, J. (2018). Design of algorithms for the automatic characterization of marine dune morphology and dynamics. Ocean, Atmosphere. ENSTA Bretagne - École nationale supérieure de techniques avancées Bretagne.

805 OpenStreetMap contributors. Planet dump retrieved from https://planet.openstreetmap.org (accessed on 23 August 2023).

Parsons, D. R., Best, J. L., Orfeo, O., Hardy, R. J., Kostaschuk, R., & Lane, S. N. (2005). Morphology and flow fields of three-dimensional dunes, Rio Paraná, Argentina: Results from simultaneous multibeam echo sounding and acoustic Doppler current profiling. Journal of Geophysical Research, 110(F4), F04S03. https://doi.org/10.1029/2004JF000231.

Raja, J., Muralikrishnan, B., Fu, S. (2002). Recent advances in separation of roughness,

810 waviness and form. Precision Engineering, 26:222-235.

Scheiber, L., & Lefebvre, A. (2023). The influence of different geometric definitions on dune characteristics. In A. Valance, T. Garlan, A. Crave, & A. Gangloff (Eds.), MARID VII: Seventh international conference on marine and river dune dynamics (pp. 293–298). University of Rennes. 1 and Shom. 344 p. ISBN: 978-2-11-139512-1.

Scheiber, L., Lojek, O., Götschenberg, A., Visscher, J., & Schlurmann, T. (2021). Robust methods for the decomposition and

815 interpretation of compound dunes applied to a complex hydromorphological setting. Earth Surface Processes and Landforms, 46(2), 478–489. https://doi.org/10.1002/esp.5040

Scheiber, L., Zomer, J., Wang, L., Cisneros, J., Gutierrez, R. R., & Lefebvre, A. (2024). Automated bedform identification—A meta-analysis of current methods and the heterogeneity of their outputs. Journal of Geophysical Research: Earth Surface, 129, e2023JF007607. https://doi.org/10.1029/2023JF007607.

820 Simons, D. B., Richardson, E. V., Nordin, C. F. (1965) Bedload equation for ripples and dunes, US Government Printing Office, Washington D.C., USA.

Ten Brinke, W.B.M., Wilbers, A.W.E., Wesseling, C. (1999): Dune growth, decay and migration rates during large-magnitude flood at sand and mixed sand-gravel bed in the Dutch Rhine river system. Special Publication of the International Association of Sedimentologists 28, 15-32.

Van der Mark, R., Blom, A. (2007). A new and widely applicable tool for determining the geometric properties of bedforms. 10.13140/RG.2.2.17637.40161.

Van Dijk, T. A. G. P., Lindenbergh, R. C., & Egberts, P. J. P. (2008). Separating bathymetric data representing multiscale rhythmic bed forms: A geostatistical and spectral method compared. Journal of Geophysical Research, 113(F4), F04017. https://doi.org/10.1029/2007JF000950.

Van Rijn, L.C. (1993). Principles of sediment transport in rivers, estuaries and coastal seas.

Van Rijn, L.C. (2007). Unified View of Sediment Transport by Currents and Waves. I: Initiation of Motion, Bed Roughness, and Bed-Load Transport. Journal of Hydraulic Engineering. 133. 10.1061/(ASCE)0733-9429(2007)133:6(649).

Venditti, J. (2013). 9.10 Bedforms in Sand-Bedded Rivers. 10.1016/B978-0-12-374739-6.00235-9.

Wang, L., Yu, Q., Zhang, Y., Flemming, B. W., Wang, Y., & Gao, S. (2020). An automated procedure to calculate the morphological parameters of superimposed rhythmic bedforms. Earth Surface Processes and Landforms, 45(14), 3496–3509. https://doi.org/10.1002/esp.4983.

Wesseling, C., Wilbers, A. W. E. (2000). Manual DT2D version 2.3: Software for dune-tracking in two dimensions. (In Dutch). Tech. rep., Faculteit der Ruimtelijke Wetenschappen, Universiteit Utrecht, Utrecht.

Wilbers, A. W. E. and Ten Brinke, W. B. M. (2003): The response of subaqueous dunes to floods in sand and gravel bed reaches of the Dutch Rhine, Sedimentology, 50, 1013–1034.

Zomer, J.Y., Naqshband, S., Hoitink, A.J.F. (2021a). Short communication: A new tool to define multiscale bedform characteristics from bed elevation data. 10.5194/esurf-2021-98.

Zomer, J.Y., Naqshband, S., Vermeulen, B., Hoitink, A.J.F. (2021b). Rapidly migrating secondary bedforms can persist on the lee of slowly migrating primary river dunes. Journal of Geophysical Research; Earth Surface, 126, e2020JF005918.

Zomer, J. Y., Vermeulen, B., and Hoitink, A. J. F. (2023). Coexistence of two dune scales in a lowland river, Earth Surf. Dynam., 11, 1283–1298, https://doi.org/10.5194/esurf-11-1283-2023, 2023.